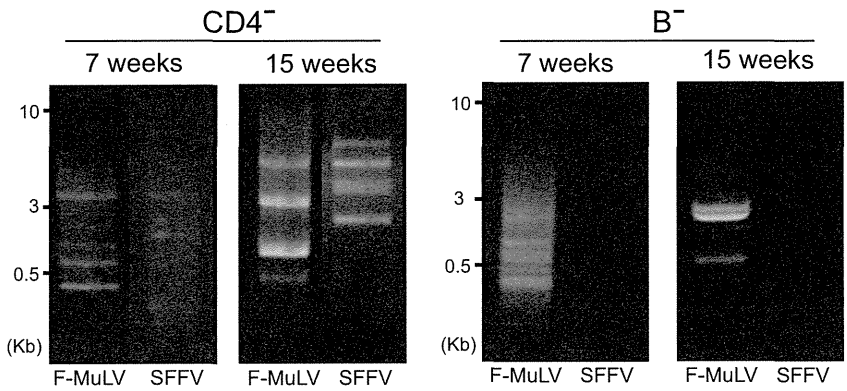

FIG 6 Changes in the clonality of virus-infected cells. Spleen cells were prepared from B6 mice lacking $CD4^+$ T cells ($CD4^-$) or B cells (B^-) at 7 weeks or at around 15 weeks after FV inoculation, and genomic DNA was purified. The host-virus junctional segments were amplified by the inverse PCR method and specific primers for F-MuLV or SFFV, and the PCR products were separated by agarose gel electrophoresis and visualized with ethidium bromide. Data shown are representative of those obtained from more than 10 individuals.

TER-119, CD3, CD11c, CD14, NK1.1, or MHC class II, on the surfaces of larger cells expanding in the spleens of FV-infected B cell-deficient mice (Fig. 9B), indicating the development of myeloid leukemia. Similarly, cells with morphological characteristics consistent with myeloid lineage with large cleaved nuclei dominated the spleens of B cell-deficient B6 mice in the pathological condition after F-MuLV inoculation and their peripheral blood contained large blastic cells with convoluted nuclei and granulocytes with hypersegmented nuclei (Fig. 9C). They also possessed in the spleens large cells with higher side scatters that were positive for F-MuLV gp70, CD11b, and Ly6G, but lacking the expression of TER-119, CD3, NK1.1, or CD14 (Fig. 9D). Thus, cellular phenotypes of large blastic cells in the spleen were essentially identical between FV-infected and F-MuLV-infected B cell-deficient B6 mice in their pathological conditions. Again, the expression of polytropic viral envelope antigens reactive with MAb 24-6 or 514 were not detectable by flow cytometric analyses of the spleen cells (data not shown). Taken together, these results indicate that persistent infection with F-MuLV induces the development of myeloid leukemia in B cell-deficient adult B6 mice, whereas persistent infection with SFFV plus F-MuLV induces predominantly erythroleukemia in adult B6 mice in the absence of $CD4^+$ T cells.

F-MuLV proviruses are not preferentially integrated at the *Fli-1* and *PU.1* loci in B cell-deficient B6 mice. Our results clearly demonstrate that FV-induced leukemia cell types were different between $CD4^+$ T cell- and B cell-deficient B6 mice. Thus, we next

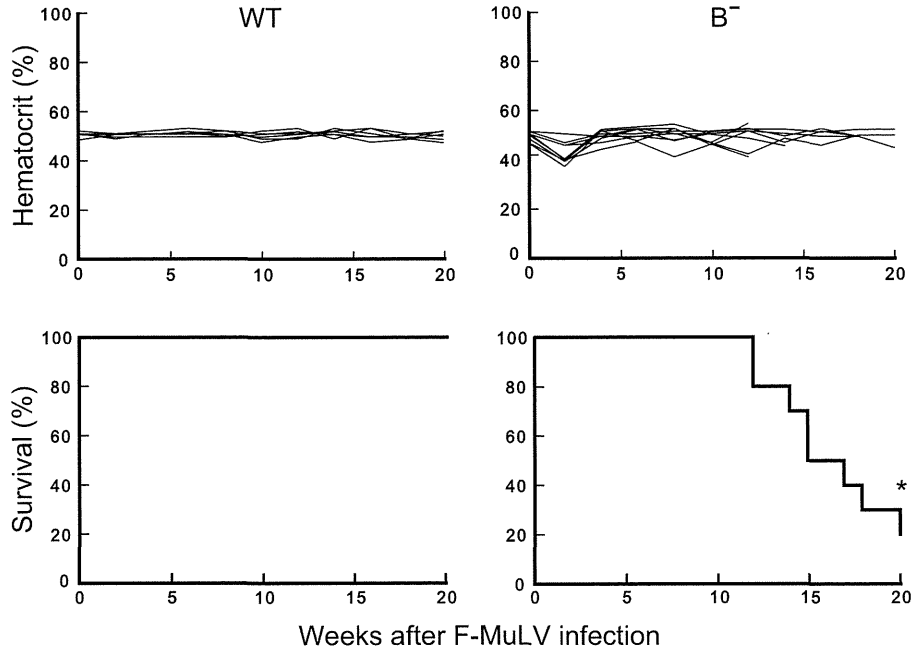

FIG 7 Survival rates and hematocrit values in B cell-deficient B6 mice upon infection with F-MuLV free of SFFV. B cell-deficient (B^-, $n = 10$) or WT B6 mice ($n = 6$) were inoculated with 5,000 focus-forming units of F-MuLV, and their survival rates and hematocrit values were analyzed. The entire set of experiments was performed twice with essentially the same results. *, significantly different from the survival curve of the WT mice ($P = 0.0040$) by Mantel-Cox test.

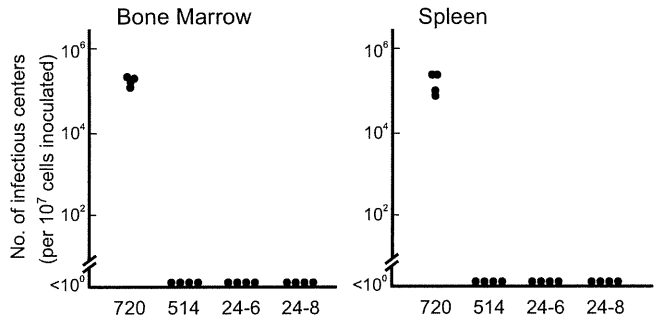

FIG 8 MCF viruses were undetectable in B6 mice lacking B cells upon F-MuLV infection. Bone marrow and spleen cells were prepared from B cell-deficient B6 mice between 14 and 17 weeks after F-MuLV inoculation and then incubated on monolayers of *Mus dunni* cells for 2 days. Foci of virus-infected cells were stained with MAb 720, which is specific for the *env* gene product of F-MuLV, MAb 514, which reacts with SFFV and some MCF viruses, and MCF virus-reactive MAbs 24-6 and 24-8 (8, 47, 49). Each circle represents the actual number of infectious centers detected from an individual mouse.

investigated the locations of the proviruses integrated into the mouse genome in leukemic mice. The host-provirus junctional segments were amplified from spleen genomic DNA by the inverse PCR method as described above (Fig. 6), and the amplified DNA segments were sequenced. In $CD4^+$ T cell-deficient B6 mice, SFFV proviruses were integrated within or near the loci of *Fli1* (in 3 out of 10 mice tested) and *PU.1* (in 4 out of the 10 mice) (Table 1), which were reported previously as major targets for integration of F-MuLV or SFFV proviruses in erythroleukemia cell lines established from FV-susceptible mice (3, 39). In addition, SFFV proviruses were integrated within the *Erg* gene locus in 2 of the 10 $CD4^+$ T cell-deficient B6 mice examined. The provirus integrations into these three gene loci were repeatedly observed, but other integration sites were each identified in only one mouse. Unexpectedly, none of the F-MuLV proviruses were integrated into *Fli1* gene locus in these $CD4^+$ T cell-deficient mice, although *Fli1* gene has been first identified as a frequent target for F-MuLV provirus integration in the FV-induced erythroleukemia cells established from FV-susceptible mice (3). In B cell-deficient B6 mice, none of F-MuLV proviruses detected were integrated into the *Fli1* or *PU.1* locus (Table 2). Instead, the actual integration sites of F-MuLV proviruses were various, and none were found repeatedly in the 10 leukemic mice examined. However, as some of the genes within or near the location where the provirus integration was observed function as transcription factors, intracellular signal transduction molecules, or regulators for cell growth/differentiation, these may be related to the leukemogenesis induced by F-MuLV infection in B cell-deficient B6 mice.

DISCUSSION

In the present study, we have shown that $Fv2^r$ B6 mice nevertheless develop polycythemia and splenomegaly followed by fatal leukemia when $CD4^+$ T cells are lacking. The expansion of TER-119^+ erythroid progenitor cells in the spleen with high level expression of F-MuLV gp70 and SFFV gp55, the progressive increase in the numbers of F-MuLV and SFFV proviral integrations in the spleen cell genome, and oligoclonal integration of both F-MuLV and SFFV proviruses in the late stage of infection all agree with the previously described cellular and molecular characteristics of FV-induced erythroleukemia that develops in $Fv2^s$-possessing susceptible mice (2, 38), although the tempos of disease development were much slower in $CD4^+$ T cell-deficient B6 mice than in $Fv2^s$-possessing mice. In fact, $Fv2^{r/s}$ $CB6F_1$ mice develop significant splenomegaly by 2 weeks after FV infection (27, 43) and severe polycythemia at as early as 3 weeks post FV infection (60), while spleen weights of $CD4^+$ T cell-deficient B6 mice at 2 weeks after FV infection were not different from those of infected WT B6 mice (data not shown). Nevertheless, the frequent involvement of the *Ets*-family *PU.1* and *Fli1* genes as SFFV integration sites indicates that the fatal leukemia observed in $CD4^+$ T cell-deficient B6 mice, despite the lack of the $Fv2^s$ allele, resembles authentic FV-induced erythroleukemia that emerges through the insertional activation of the transcription factors in proliferating erythroid cells (3, 39, 45). Further, another *Ets*-family gene encoding the transcription factor Erg was shown to be involved in SFFV proviral integration in the present study. The *Erg* locus was identified in a previous report as a proviral integration site in B6 mice injected as neonates with F-MuLV in association with the development of myeloid leukemia (65). Further, *Erg* has recently been shown to induce erythro-megakaryocytic leukemia upon hematopoietic cell-specific overexpression (7). Collectively, these data indicate that the erythroleukemia induced with FV in $CD4^+$ T cell-deficient B6 mice is indeed similar to the classical Friend disease in its molecular pathogenesis.

On the other hand, the fatal pathology that developed in B cell-deficient B6 mice differs from previously described Friend disease as the pathology developed without preceding polycythemia and splenomegaly, and neither the expression of SFFV gp55 on erythroid cells nor oligoclonal integration of SFFV proviruses was observed. The disease rather resembles leukemia that develops after a long latency period upon neonatal inoculation of F-MuLV, as both diseases develop independently of SFFV. In fact, neonatal inoculation of C57BL/10 or B6 mice with F-MuLV has been shown to induce differentiated (granulocytic) or undifferentiated myeloid leukemia (10, 55). It has been generally accepted that during ongoing ecotropic murine leukemia virus infection the emergence of recombinant MCF viruses that can utilize a different receptor and show an altered tissue tropism markedly increase the chances of insertional gene activation, ultimately resulting in the development of oligoclonal leukemia (16, 64). In the case of B cell-deficient B6 mice, however, leukemia developed through oligoclonal integration of F-MuLV itself without the emergence of infectious MCF viruses detectable with currently used MAb. Interestingly, a similar lack of the generation of MCF viruses has also been reported in C57BL mice neonatally infected with F-MuLV (10, 55). Although we cannot exclude the possibility that recombinant viruses not detectable with the MAb we used were generated, it is possible that in the absence of B cells and thus a lack of virus-neutralizing Ab, rapid and uncontrolled replication of ecotropic F-MuLV alone can result in a leukemogenic promoter insertion.

It has recently been shown that in B6 mice with a range of immunodeficiencies commonly affecting Ab-producing functions, spontaneous activation of a replication-defective, endogenous ecotropic murine leukemia retrovirus, Emv2, results in the emergence of infectious recombinant viruses, and the resultant viremia leads to the development of lymphocytic leukemia/lymphoma in aged animals (66, 67). However, the spontaneous tumor development started to be observed after 6 months of age in Rag1-deficient B6 mice (66), and mortality started after 40 weeks of age

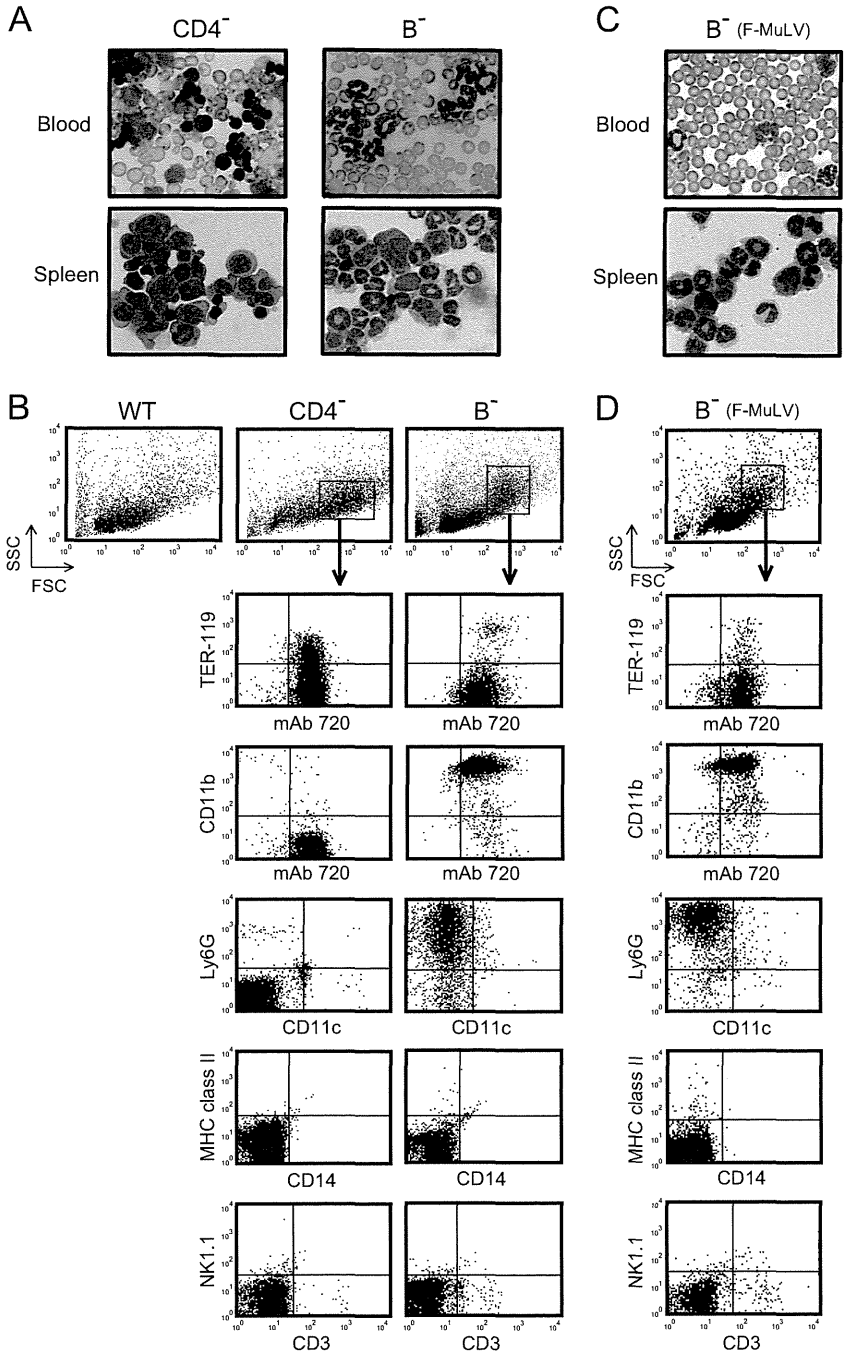

FIG 9 Expansion of myeloid cells in B cell-deficient B6 mice upon FV or F-MuLV infection. (A) Representative peripheral blood smear specimens (upper panels) and cytospin preparations of the spleen cells (lower panels) from $CD4^+$ T cell- or B cell-deficient B6 mice prepared between 12 and 17 weeks after FV infection and stained with May-Grunwald Giemsa stain (all photographs were taken at the same magnification). (B) Cell populations expanded in the spleen of each infected mouse were gated as indicated and analyzed for the expression of the surface molecules by flow cytometry. Similar data were obtained in the analyses of more than 5 individuals per group. (C) Representative peripheral blood smear and cytospin preparation of the spleens from B cell-deficient B6 mice between 14 and 17 weeks after F-MuLV inoculation (May-Grunwald Giemsa stain). Note the large myeloid cells of different differentiation stages, similar to those observed in FV-infected B cell-deficient B6 mice in the spleen, and the appearance of immature myeloid cells with convoluted nuclei and granulocytes with hypersegmented nuclei in the peripheral blood. (D) Flow cytometric analyses of cells expanded in the spleens of F-MuLV-infected, B cell-deficient B6 mice. Representative dot plots from an individual mouse are shown. Similar data were obtained from 6 individuals.

in *Tlr3*, *Tlr7*, *Tlr9* triple-knockout B6 mice (67). On the other hand, we inoculated $CD4^+$ T cell- or B cell-deficient B6 mice with FV or F-MuLV at 7–8 weeks, and the infected animals started to show mortality at around 10 weeks after infection (≤18 weeks in age) and most died by 20 weeks after infection (≤28 weeks of age), well before the reported onset of spontaneous lymphoma/lymphoid leukemia. Further, the tumor cells growing in the immunodeficient B6 mice with Emv2-related viremia are reported to be $CD3^+$ and strongly express terminal deoxynucleotidyl transferase (TdT) (67), while the cells expanding in FV- or F-MuLV-infected,

TABLE 1 Integration sites of F-MuLV and SFFV in CD4$^+$ T cell-deficient B6 mice[a]

Provirus	Locus[c]	Chr[c]	Gene ID[c]	Definition or function[c]	Provirus location[d]
SFFV	*Fli1*[b]	9	14247	Transcription	0.7–2 kb up
	PU.1 (*Sfpi1*)[b]	2	20375	Transcription	Intron 1 or 12 kb up
	Erg[b]	16	13876	Transcriptional regulator	Intron 3
	Myo6, *Impg1*	9	17920, 63859	Myosin, Receptor	2 kb down, 0.1 kb down, respectively
	Ddx3	x	13205	Helicase	40 kb up
	Lbp1	19	16825	Transcriptional regulator	Intron 1
	Myb	10	17863	Transcription	23 kb up
	ADARB2	13	94191	RNA-editing deaminase	Intron 3
	Tecr	8	106529	Oxidoreductase	5 kb up
	Spns3	11	77577	Lipid transporter	2 kb up
	Top3b	16	21976	Topoisomerase	8 kb up
	Gorasp2	2	70231	Golgi complex organization	35 kb up
	Zfp219	14	69890	DNA binding	2 kb up
F-MuLV	*Bcl11a*	11	14025	Zinc finger	Intron 2
	Zfat	15	380993	Zinc finger	20 kb down
	Rabgap1l	1	29809	GTPase	Intron 20
	Grb2	11	14784	Signal	15 kb up
	Ikzf1 (*Ikaros*)	11	22778	Transcription	Intron 3
	Ath1	7	212974	Trehalase	0.1 kb down
	Pabpc1, *Snx31*	15	18458, 66696	Poly(A) binding, lipid binding	11 kb down, 27 kb up, respectively
	Ccdc83	7	75338	Unknown	Intron 6

[a] Integration sites of F-MuLV or SFFV in the spleen cell genome were determined in 10 leukemic mice by inverse PCR (Fig. 6) and sequencing of each amplified DNA band.
[b] The three gene loci were found in more than 2 mice out of 10 leukemic individuals examined, whereas the involvement of other genes was found in only a single mouse.
[c] The chromosome locus, gene ID, and putative function of the potential target genes are shown. Gene IDs are those given at the National Center for Biotechnology Information (NCBI) Gene site (http://www.ncbi.nlm.nih.gov/gene/).
[d] Proviruses were located within the indicated intron or near the potential target genes. To determine the location of proviruses integrated outside of previously identified gene loci, upstream distances from the transcription start site (up) or downstream distances from the polyadenylation signal (down) of the neighboring genes were calculated.

B cell-deficient B6 mice were CD3$^-$ and exhibited cytological and flow cytometric characteristics of myeloid cells. The large-sized blastic cells we observed in B cell-deficient B6 mice also expressed F-MuLV gp70 detectable with MAb 720, which is known to react only with F-MuLV and a limited range of recombinant viruses that harbor a C-terminal segment of gp70 derived from ecotropic F-MuLV (49). It should be noted that Emv2-related infectious retroviruses emerged spontaneously in immunodeficient B6 mice were detected with MAb 83A25 (15) which exhibits a range of reactivities reciprocal to that of MAb 720. Thus, MAb 83A25 detects all known mouse retroviruses except F-MuLV and its recombinants that harbor the C-terminal segment of F-MuLV gp70 (15, 49), and MAb 720 is unlikely to react with Emv2-derived recombinant viruses. Further, if Emv2-related infectious ecotropic viruses were produced in the spleens of B cell-deficient B6 mice we examined, such viruses likely would have been detected with MAb 24-8 in infectious center assays. Therefore, the observed development of erythroleukemia and myeloid malignancy in CD4$^+$ T cell- and B cell-deficient B6 mice, respectively, is most likely FV-induced and independent of the reported spontaneous emergence of Emv2-related retrovirus.

It is of particular interest that when NK and/or CD8$^+$ T cells were depleted, some B cell-deficient B6 mice developed polycythemia with a progressive increase in SFFV proviral integration. This indicates that in *Fv2*^{r} B6 mice SFFV-infected cells are not only restricted in their growth due to the lack of sf-Stk, but are actively eliminated in the very early phase of FV infection through cellular, but not humoral, immune responses. This is consistent with the previous findings that *Fv2*^{r}-associated resistance to FV infection did not operate in the absence of T-lymphocytes (19, 28, 63). However, the simple absence of CD8$^+$ T cells alone did not result in the development of polycythemia and did not largely affect the resistance to the disease development in B6 mice as we have shown in the present study with LDV-free FV. Thus, in CD8$^+$ T cell-deficient mice other effector mechanisms must be compensating for the lacking CTLs in eliminating SFFV-infected cells. It should be noted that CD4$^+$ T cell responses are operational in CD8$^+$ T cell-deficient mice, and the priming of CD4$^+$ T cells with an FV-derived epitope can protect highly susceptible CB6F$_1$ mice from FV-induced leukemia development in the absence of CD8$^+$ T cells (27), indicating the actual presence and effectiveness of an FV-eliminating effector mechanism other than CD8$^+$ T cells that is under the control of CD4$^+$ T cells. In this regard, it is also noteworthy that the FV-specific priming and reactivation of CD4$^+$ T cells were not severely affected in B cell-deficient mice (27). Further, activation of both CD8$^+$ effecter T cells and NK cells upon pathogen invasion are known to depend on CD4$^+$ T cells, as CD4$^+$ T cells are required for the induction of CD8$^+$ effector cells (1, 4, 48, 53) and NK cell activation upon pathogen infection is shown to be induced in the presence of CD4$^+$ effector T cells (6, 22). In addition, CD4$^+$ T cells themselves may act as cytotoxic effector cells in eliminating FV-infected target cells (24). Thus, it is conceivable that NK cells and CD8$^+$ effector T cells, as well as CD4$^+$ cytotoxic cells, are eliminating SFFV-infected cells in WT and B cell-deficient B6 mice, while these are not activated in CD4$^+$ T cell-deficient mice. In CD8$^+$ T cell-deficient mice, the SFFV eliminating function is probably exerted by NK and CD4$^+$ effector T cells.

It has been widely accepted that the interaction of SFFV gp55 with erythropoietin (Epo) receptor is required for Epo-independent differentiation of erythroid progenitor cells and the resultant polycythemia, while sf-Stk-associated signaling is required for

TABLE 2 Integration sites of F-MuLV in B cell-deficient B6 mice[a]

Provirus	Locus[b]	Chr[b]	Gene ID[b]	Definition or function[b]	Provirus location[c]
F-MuLV	*Ski*	4	20481	Chromatin binding, enzyme regulator enzyme	Intron 1
	Sox-4	13	20677	Transcription	Intron 1
	Nfu1	6	56748	Iron ion binding	Intron 1
	Ahi1	10	52906	Protein binding	Intron 19
	Hexokinase II	6	15277	Catalytic activity	Intron 1
	GATA-1	x	14460	Transcription	Intron 1
	Gpr142	11	217302	G-protein-coupled receptor activity	8 kb down
	Cdk-like 4	17	381113	Cell cycle	10 kb down
	Arpc5-like	2	74192	Actin binding	Intron 1
	Zbp1	2	58203	DNA binding	Intron 1
	Dnahc6	6	330355	ATP binding	4 kb down
	Gimap5	6	317757	GTPase	Intron 1
	Ntn1, STX8	11	18208, 55943	Protein binding, ubiqutin protein ligase binding	5 kb down
	Mc2r	18	17200	Corticotrophin receptor	40 kb up
	Cdh23	10	22295	Calcium ion binding	Intron 3
	Egfl7, Notch1	2	353156, 18128	Calcium ion binding, chromatin DNA binding	28 kb up, 48 kb up, respectively
	Lrrc25, Ssbp4	8	211228, 76900	Unknown, DNA binding	1 kb up, 9 kb up, respectively
	Prkar2a	9	19087	cAMP binding	Intron 1
	Fchsd2	7	207278	Unknown	43 kb up
	Sfrs3	17	20383	Splicing factor	35 kb down
	Igf1r	7	16001	Receptor	Intron 1
	Smad 3	9	17127	Transcription	28 kb up

[a] Integration sites of F-MuLV were determined in 10 leukemic mice by inverse PCR (Fig. 6) and sequencing of each amplified DNA band. All of the target genes were found in only a single mouse analyzed.
[b] Chromosome locus, gene ID, and putative function of the potential target genes are shown. Gene IDs are those given at the NCBI Gene site (http://www.ncbi.nlm.nih.gov/gene).
[c] Proviruses were located within the indicated intron or near the potential target genes. To determine the location of proviruses integrated outside of previously identified gene loci, upstream distances from the transcription start site (up) or downstream distances from the polyadenylation signal (down) of the neighboring genes were calculated.

Epo-independent proliferation (12, 68). As FV-induced erythroleukemia is suggested to develop through 2 stages, which are promotion of erythroid cell proliferation and the blockade of their differentiation (2, 12, 21, 38, 57, 68), one would wonder what caused erythroid cell proliferation prior to the putative secondary step of *PU.1* or *Fli1* activation in $CD4^+$ T cell-deficient B6 mice in the absence of sf-Stk. However, a slow development of erythroleukemia similar to what we observed in $CD4^+$ T cell-deficient B6 mice has been observed in *Fv2*^{r} mice with a mutant FV that encodes an SFFV *env* gene product, gp42, with a deletion in the membrane-proximal domain (31, 34). As intracellular signaling pathways are largely overlapping between gp55-Epo-receptor and gp55-sf-Stk interactions (12), FV infection of *Fv2*^{r} mice may induce sf-Stk-independent growth of erythroid cells that is slow but enough to function as the first stage of leukemogenesis.

Altogether, the present study has provided several new insights into the pathogenesis of FV-induced leukemia and the *Fv2*-associated resistance to it. The *Fv2*^{r} allele operates through the lack of expression of sf-Stk (46), but does not provide complete resistance to SFFV-induced erythroid cell proliferation as previously pointed out (19, 28, 31, 34, 63). Rather, SFFV-infected cells are eliminated by cellular immune responses to which $CD4^+$ T cells are indispensable. In the absence of B cells, the SFFV component of FV is eliminated as quickly as in WT mice in the presence of the homozygous *FV2*^{r} allele, but the remaining F-MuLV alone can induce fatal myeloid leukemia possibly without requiring the emergence of recombinant MCF viruses. These new observations may also contribute to the understanding of quantitative and kinetic aspects of retrovirus-induced multistep leukemogenesis, as future studies may pinpoint critical steps at which cellular immune responses control the emergence of SFFV-induced leukemia stem cells (21, 43, 57) and Ab responses restrict the emergence of F-MuLV-induced ones.

ACKNOWLEDGMENTS

Animal experiments were supported by members of the Central Research Facilities, Kinki University Faculty of Medicine. We thank J. B. Dowell for critical reading and correction of the manuscript.

This work was supported in part by Grants-in-Aid for Scientific Research (KAKENHI) from the Ministry of Education, Culture, Sports, Science and Technology of Japan, including the Anti-Aging Center Project, and from the Ministry of Health, Labor and Welfare of Japan for research on HIV/AIDS.

REFERENCES

1. **Ahmed KA, Wang L, Munegowda MA, Mulligan SJ, Gordon JR, Griebel P, Xiang J.** 2012. Direct in vivo evidence of $CD4^+$ T cell requirement for CTL response and memory via pMHC-I targeting and CD40L signaling. J. Leukoc. Biol. **92**:289–300.
2. **Ben-David Y, Bernstein A.** 1991. Friend virus-induced erythroleukemia and the multistage nature of cancer. Cell **66**:831–834.
3. **Ben-David Y, Giddens EB, Bernstein A.** 1990. Identification and mapping of a common proviral integration site *Fli-1* in erythroleukemia cells induced by Friend murine leukemia virus. Proc. Natl. Acad. Sci. U. S. A. **87**:1332–1336.
4. **Bennett SR, Carbone FR, Karamalis F, Flavell RA, Miller JF, Heath WR.** 1998. Help for cytotoxic-T-cell responses is mediated by CD40 signalling. Nature **393**:478–480.
5. **Best S, Le Tissier P, Towers G, Stoye JP.** 1996. Positional cloning of the mouse retrovirus restriction gene *Fv1*. Nature **382**:826–829.
6. **Bihl F, Pecheur J, Breart B, Poupon G, Cazareth J, Julia V, Glaichenhaus N, Braud VM.** 2010. Primed antigen-specific $CD4^+$ T cells are required for NK cell activation in vivo upon *Leishmania major* infection. J. Immunol. **185**:2174–2181.
7. **Carmichael CL, Metcalf D, Henley KJ, Kruse EA, Di Rago L, Mifsud S, Alexander WS, Kile BT.** 2012. Hematopoietic overexpression of the tran-

scription factor Erg induces lymphoid and erythro-megakaryocytic leukemia. Proc. Natl. Acad. Sci. U. S. A. **109**:15437–15442.
8. **Chesebro B, Britt W, Evans L, Wehrly K, Nishio J, Cloyd M.** 1983. Characterization of monoclonal antibodies reactive with murine leukemia viruses: use in analysis of strains of Friend MCF and Friend ecotropic murine leukemia virus. Virology **127**:134–148.
9. **Chesebro B, Miyazawa M, Britt WJ.** 1990. Host genetic control of spontaneous and induced immunity to Friend murine retrovirus infection. Annu. Rev. Immunol. **8**:477–499.
10. **Chesebro B, Portis JL, Wehrly K, Nishio J.** 1983. Effect of murine host genotype on MCF virus expression, latency, and leukemia cell type of leukemias induced by Friend murine leukemia helper virus. Virology **128**: 221–233.
11. **Chesebro B, Wehrly K.** 1979. Identification of a non-H-2 gene (*Rfv-3*) influencing recovery from viremia and leukemia induced by Friend virus complex. Proc. Natl. Acad. Sci. U. S. A. **76**:425–429.
12. **Cmarik J, Ruscetti S.** 2010. Friend spleen focus-forming virus activates the tyrosine kinase sf-Stk and the transcription factor PU.1 to cause a multi-stage erythroleukemia in mice. Viruses **2**:2235–2257.
13. **Deeks SG, Walker BD.** 2007. Human immunodeficiency virus controllers: mechanisms of durable virus control in the absence of antiretroviral therapy. Immunity **27**:406–416.
14. **Dittmer U, He H, Messer RJ, Schimmer S, Olbrich AR, Ohlen C, Greenberg PD, Stromnes IM, Iwashiro M, Sakaguchi S, Evans LH, Peterson KE, Yang G, Hasenkrug KJ.** 2004. Functional impairment of CD8(+) T cells by regulatory T cells during persistent retroviral infection. Immunity **20**:293–303.
15. **Evans LH, Morrison RP, Malik FG, Portis J, Britt WJ.** 1990. A neutralizable epitope common to the envelope glycoproteins of ecotropic, polytropic, xenotropic, and amphotropic murine leukemia viruses. J. Virol. **64**:6176–6183.
16. **Fan H.** 1997. Leukemogenesis by Moloney murine leukemia virus: a multistep process. Trends Microbiol. **5**:74–82.
17. **Friend C.** 1957. Cell-free transmission in adult Swiss mice of a disease having the character of a leukemia. J. Exp. Med. **105**:307–318.
18. **Gerlach N, Schimmer S, Weiss S, Kalinke U, Dittmer U.** 2006. Effects of type I interferons on Friend retrovirus infection. J. Virol. **80**:3438–3444. (Erratum, 81:6160, 2007.)
19. **Hasenkrug KJ.** 1999. Lymphocyte deficiencies increase susceptibility to Friend virus-induced erythroleukemia in *Fv-2* genetically resistant mice. J. Virol. **73**:6468–6473.
20. **Hasenkrug KJ, Valenzuela A, Letts VA, Nishio J, Chesebro B, Frankel WN.** 1995. Chromosome mapping of *Rfv3*, a host resistance gene to Friend murine retrovirus. J. Virol. **69**:2617–2620.
21. **Hegde S, Hankey P, Paulson RF.** 2012. Self-renewal of leukemia stem cells in Friend virus-induced erythroleukemia requires proviral insertional activation of Spi1 and hedgehog signaling but not mutation of p53. Stem Cells. **30**:121–130.
22. **Horowitz A, Behrens RH, Okell L, Fooks AR, Riley EM.** 2010. NK cells as effectors of acquired immune responses: effector $CD4^+$ T cell-dependent activation of NK cells following vaccination. J. Immunol. **185**: 2808–2818.
23. **Ikeda H, Laigret F, Martin MA, Repaske R.** 1985. Characterization of a molecularly cloned retroviral sequence associated with *Fv-4* resistance. J. Virol. **55**:768–777.
24. **Iwanami N, Niwa A, Yasutomi Y, Tabata N, Miyazawa M.** 2001. Role of natural killer cells in resistance against Friend retrovirus-induced leukemia. J. Virol. **75**:3152–3163.
25. **Kabat D.** 1989. Molecular biology of Friend viral erythroleukemia. Curr. Top. Microbiol. Immunol. **148**:1–42.
26. **Kanari Y, Clerici M, Abe H, Kawabata H, Trabattoni D, Caputo SL, Mazzotta F, Fujisawa H, Niwa A, Ishihara C, Takei YA, Miyazawa M.** 2005. Genotypes at chromosome 22q12-13 are associated with HIV-1-exposed but uninfected status in Italians. AIDS **19**:1015–1024.
27. **Kawabata H, Niwa A, Tsuji-Kawahara S, Uenishi H, Iwanami N, Matsukuma H, Abe H, Tabata N, Matsumura H, Miyazawa M.** 2006. Peptide-induced immune protection of $CD8^+$ T cell-deficient mice against Friend retrovirus-induced disease. Int. Immunol. **18**:183–198.
28. **Kitagawa M, Matsubara O, Kasuga T.** 1986. Dynamics of lymphocytic subpopulations in Friend leukemia virus-induced leukemia. Cancer Res. **46**:3034–3039.
29. **Kitamura D, Roes J, Kuhn R, Rajewsky K.** 1991. A B cell-deficient mouse by targeted disruption of the membrane exon of the immunoglobulin μ chain gene. Nature **350**:423–426.
30. **Koller BH, Marrack P, Kappler JW, Smithies O.** 1990. Normal development of mice deficient in β_2M, MHC class I proteins, and $CD8^+$ T cells. Science **248**:1227–1230.
31. **Kozak SL, Hoatlin ME, Ferro FE, Jr, Majumdar MK, Geib RW, Fox MT, Kabat D.** 1993. A Friend virus mutant that overcomes *Fv-2*^{rr} host resistance encodes a small glycoprotein that dimerizes, is processed to cell surfaces, and specifically activates erythropoietin receptors. J. Virol. **67**: 2611–2620.
32. **Li J, Hakata Y, Takeda E, Liu Q, Iwatani Y, Kozak CA, Miyazawa M.** 2012. Two genetic determinants acquired late in *mus* evolution regulate the inclusion of exon 5, which alters mouse APOBEC3 translation efficiency. PLoS Pathog. **8**(1):e1002478. doi:10.1371/journal.ppat.1002478.
33. **Lilly F.** 1970. *Fv-2*: identification and location of a second gene governing the spleen focus response to Friend leukemia virus in mice. J. Natl. Cancer Inst. **45**:163–169.
34. **Majumdar MK, Cho CL, Fox MT, Eckner KL, Kozak S, Kabat D, Geib RW.** 1992. Mutations in the *env* gene of Friend spleen focus-forming virus overcome *Fv-2*^{r}-mediated resistance to Friend virus-induced erythroleukemia. J. Virol. **66**:3652–3660.
35. **Miyazawa M, Fujisawa R, Ishihara C, Takei YA, Shimizu T, Uenishi H, Yamagishi H, Kuribayashi K.** 1995. Immunization with a single T helper cell epitope abrogates Friend virus-induced early erythroid proliferation and prevents late leukemia development. J. Immunol. **155**:748–758.
36. **Miyazawa M, Nishio J, Wehrly K, Chesebro B.** 1992. Influence of MHC genes on spontaneous recovery from Friend retrovirus-induced leukemia. J. Immunol. **148**:644–647.
37. **Miyazawa M, Tsuji-Kawahara S, Kanari Y.** 2008. Host genetic factors that control immune responses to retrovirus infections. Vaccine **26**:2981–2996.
38. **Moreau-Gachelin F.** 2008. Multi-stage Friend murine erythroleukemia: molecular insights into oncogenic cooperation. Retrovirology **5**:99.
39. **Moreau-Gachelin F, Tavitian A, Tambourin P.** 1988. *Spi-1* is a putative oncogene in virally induced murine erythroleukaemias. Nature **331**:277–280.
40. **Nagase H, Wang CR, Yoshimoto T, Sugishita C, Shiroishi T, Matsuzawa A, Nariuchi H.** 1998. Novel mutant mice secreting soluble CD4 without expression of membrane-bound CD4. Eur. J. Immunol. **28**:403–412.
41. **Ney PA, D'Andrea AD.** 2000. Friend erythroleukemia revisited. Blood **96**:3675–3680.
42. **O'Connell KA, Bailey JR, Blankson JN.** 2009. Elucidating the elite: mechanisms of control in HIV-1 infection. Trends Pharmacol. Sci. **30**: 631–637.
43. **Ogawa T, Tsuji-Kawahara S, Yuasa T, Kinoshita S, Chikaishi T, Takamura S, Matsumura H, Seya T, Saga T, Miyazawa M.** 2011. Natural killer cells recognize Friend retrovirus-infected erythroid progenitor cells through NKG2D-RAE-1 interactions *in vivo*. J. Virol. **85**:5423–5435.
44. **Pantaleo G, Fauci AS.** 1995. New concepts in the immunopathogenesis of HIV infection. Annu. Rev. Immunol. **13**:487–512.
45. **Paul R, Schuetze S, Kozak SL, Kabat D.** 1989. A common site for immortalizing proviral integrations in Friend erythroleukemia: molecular cloning and characterization. J. Virol. **63**:4958–4961.
46. **Persons DA, Paulson RF, Loyd MR, Herley MT, Bodner SM, Bernstein A, Correll PH, Ney PA.** 1999. *Fv2* encodes a truncated form of the Stk receptor tyrosine kinase. Nat. Genet. **23**:159–165.
47. **Portis JL, McAtee FJ, Cloyd MW.** 1982. Monoclonal antibodies to xenotropic and MCF murine leukemia viruses derived during the graft-versus-host reaction. Virology **118**:181–190.
48. **Ridge JP, Di Rosa F, Matzinger P.** 1998. A conditioned dendritic cell can be a temporal bridge between a $CD4^+$ T-helper and a T-killer cell. Nature **393**:474–478.
49. **Robertson MN, Miyazawa M, Mori S, Caughey B, Evans LH, Hayes SF, Chesebro B.** 1991. Production of monoclonal antibodies reactive with a denatured form of the Friend murine leukemia virus gp70 envelope protein: use in a focal infectivity assay, immunohistochemical studies, electron microscopy and western blotting. J. Virol. Methods **34**:255–271.
50. **Robertson SJ, Ammann CG, Messer RJ, Carmody AB, Myers L, Dittmer U, Nair S, Gerlach N, Evans LH, Cafruny WA, Hasenkrug KJ.** 2008. Suppression of acute anti-Friend virus $CD8^+$ T-cell responses by coinfection with lactate dehydrogenase-elevating virus. J. Virol. **82**:408–418.
51. **Rodriguez M, Sriram S.** 1988. Successful therapy of Theiler's virus-

induced demyelination (DA strain) with monoclonal anti-Lyt-2 antibody. J. Immunol. **140**:2950–2955.
52. **Santiago ML, Montano M, Benitez R, Messer RJ, Yonemoto W, Chesebro B, Hasenkrug KJ, Greene WC.** 2008. *Apobec3* encodes *Rfv3*, a gene influencing neutralizing antibody control of retrovirus infection. Science **321**:1343–1346.
53. **Schoenberger SP, Toes RE, van der Voort EI, Offringa R, Melief CJ.** 1998. T-cell help for cytotoxic T lymphocytes is mediated by CD40-CD40L interactions. Nature **393**:480–483.
54. **Shibuya T, Mak TW.** 1982. Host control of susceptibility to erythroleukemia and to the types of leukemia induced by Friend murine leukemia virus: initial and late stages. Cell **31**:483–493.
55. **Silver J.** 1984. Role of mink cell focus-inducing virus in leukemias induced by Friend ecotropic virus. J. Virol. **50**:872–877.
56. **Sitbon M, Sola B, Evans L, Nishio J, Hayes SF, Nathanson K, Garon CF, Chesebro B.** 1986. Hemolytic anemia and erythroleukemia, two distinct pathogenic effects of Friend MuLV: mapping of the effects to different regions of the viral genome. Cell **47**:851–859.
57. **Subramanian A, Hegde S, Porayette P, Yon M, Hankey P, Paulson RF.** 2008. Friend virus utilizes the BMP4-dependent stress erythropoiesis pathway to induce erythroleukemia. J. Virol. **82**:382–393.
58. **Suzuki T, Shen H, Akagi K, Morse HC, Malley JD, Naiman DQ, Jenkins NA, Copeland NG.** 2002. New genes involved in cancer identified by retroviral tagging. Nat. Genet. **32**:166–174.
59. **Takamura S, Tsuji-Kawahara S, Yagita H, Akiba H, Sakamoto M, Chikaishi T, Kato M, Miyazawa M.** 2010. Premature terminal exhaustion of Friend virus-specific effector $CD8^+$ T cells by rapid induction of multiple inhibitory receptors. J. Immunol. **184**:4696–4707.
60. **Takeda E, Tsuji-Kawahara S, Sakamoto M, Langlois MA, Neuberger MS, Rada C, Miyazawa M.** 2008. Mouse APOBEC3 restricts friend leukemia virus infection and pathogenesis *in vivo*. J. Virol. **82**:10998–11008.
61. **Tsuji-Kawahara S, Chikaishi T, Takeda E, Kato M, Kinoshita S, Kajiwara E, Takamura S, Miyazawa M.** 2010. Persistence of viremia and production of neutralizing antibodies differentially regulated by polymorphic *APOBEC3* and *BAFF-R* loci in friend virus-infected mice. J. Virol. **84**:6082–6095.
62. **Tsuruyama T, Nakamura T, Jin G, Ozeki M, Yamada Y, Hiai H.** 2002. Constitutive activation of Stat5a by retrovirus integration in early pre-B lymphomas of SL/Kh strain mice. Proc. Natl. Acad. Sci. U. S. A. **99**:8253–8258.
63. **Van der Gaag HC, Axelrad AA.** 1990. Friend virus replication in normal and immunosuppressed C57BL/6 mice. Virology **177**:837–839.
64. **Wensel DL, Li W, Cunningham JM.** 2003. A virus-virus interaction circumvents the virus receptor requirement for infection by pathogenic retroviruses. J. Virol. **77**:3460–3469.
65. **Yatsula B, Galvao C, McCrann M, Perkins AS.** 2006. Assessment of F-MuLV-induced tumorigenesis reveals new candidate tumor genes including *Pecam1*, *St7*, and *Prim2*. Leukemia **20**:162–165.
66. **Young GR, Eksmond U, Salcedo R, Alexopoulou L, Stoye JP, Kassiotis G.** 2012. Resurrection of endogenous retroviruses in antibody-deficient mice. Nature **491**:774–778.
67. **Yu P, Lubben W, Slomka H, Gebler J, Konert M, Cai C, Neubrandt L, Prazeres da Costa O, Paul S, Dehnert S, Dohne K, Thanisch M, Storsberg S, Wiegand L, Kaufmann A, Nain M, Quintanilla-Martinez L, Bettio S, Schnierle B, Kolesnikova L, Becker S, Schnare M, Bauer S.** 2012. Nucleic acid-sensing Toll-like receptors are essential for the control of endogenous retrovirus viremia and ERV-induced tumors. Immunity **37**:867–879.
68. **Zhang J, Randall MS, Loyd MR, Li W, Schweers RL, Persons DA, Rehg JE, Noguchi CT, Ihle JN, Ney PA.** 2006. Role of erythropoietin receptor signaling in Friend virus-induced erythroblastosis and polycythemia. Blood **107**:73–78.

Journal of Medicinal Chemistry

Article

pubs.acs.org/jmc

Crystal Structures of Hereditary Vitamin D-Resistant Rickets-Associated Vitamin D Receptor Mutants R270L and W282R Bound to 1,25-Dihydroxyvitamin D_3 and Synthetic Ligands

Makoto Nakabayashi,*[,†,‡,∥] Yoshito Tsukahara,[†] Yukiko Iwasaki-Miyamoto,[‡] Mika Mihori-Shimazaki,[‡] Sachiko Yamada,*[,‡,∥] Satomi Inaba,[⊥] Masayuki Oda,[⊥] Masato Shimizu,[†,‡] Makoto Makishima,[∥] Hiroaki Tokiwa,[#] Teikichi Ikura,[§] and Nobutoshi Ito[§]

[†]Graduate School of Biomedical Science, [‡]Institute of Biomaterials and Bioengineering, and [§]Medical Research Institute, Tokyo Medical and Dental University, Bunkyo-ku, Tokyo 113-8510, Japan

[∥]Department of Biomedical Sciences, Nihon University School of Medicine, Itabashi-ku, Tokyo 173-8610, Japan

[⊥]Graduate School of Life and Environmental Sciences, Kyoto Prefectural University, Sakyo-ku, Kyoto 606-8522, Japan

[#]Department of Chemistry, Faculty of Science, Rikkyo University, Toshima-ku, Tokyo 171-8501, Japan

Supporting Information

ABSTRACT: The vitamin D receptor (VDR), a member of the nuclear receptor superfamily, functions as a ligand-dependent transcription factor for various genes. Hereditary vitamin D-resistant rickets (HVDRR), an autosomal recessive disease, is caused by mutations in the VDR. In particular, the missense mutations R274L and W286R in the ligand-binding domain of the VDR can severely reduce or even eliminate natural hormone responsiveness. Here, we report a crystal structure analysis of the R270L and W282R mutants of rat VDR (human R274L and W286R, respectively) in complex with the natural hormone and synthetic ligands. We also studied the folding properties of the mutant proteins by using circular dichroism spectra. Our study indicates that these mutations result in only local structural modifications. We discuss why these mutations disrupt the VDR function and provide clues to develop effective ligands for the treatment of HVDRR.

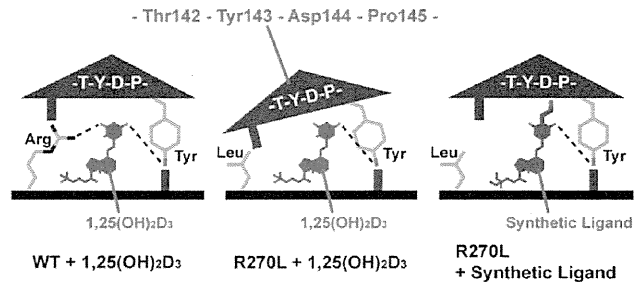

INTRODUCTION

Vitamin D_3 is acquired from dietary sources or via ultraviolet irradiation of 7-dehydrocholesterol in the epidermis. It is metabolized to its active hormonal form, 1,25-dihydroxyvitamin D_3 [$1,25(OH)_2D_3$] via the action of D_3 1α-hydrdoxylase (CYP27B1) expressed predominantly in the kidney.[1] $1,25\text{-}(OH)_2D_3$ maintains calcium and phosphorus homeostasis in vertebrates[2] by directly binding to the vitamin D receptor (VDR)[3] in the intestine, kidney, and bone. This activity is regulated via feedback inhibition of parathyroid hormone production in the parathyroid glands. $1,25(OH)_2D_3$ is also produced locally in numerous cell types that express the VDR, notably skin, cells of the immune system, colon, pancreas, and vasculature.[4] The significance of the local extraosseous effects of $1,25(OH)_2D_3$ is not fully understood, but it appears that vitamin D, likely cooperating with other regulators, exerts immunoregulation, antimicrobial defense, xenobiotic detoxification, anticancer actions, control of insulin secretion, and, possibly, cardiovascular benefits.[5]

When vitamin D binds to the VDR, it changes its conformation to the active form and interacts with the 9-*cis*-retinoic acid receptor (RXR) forming a heterodimer.[6] The VDR/RXR heterodimer binds to vitamin D-responsive elements (VDRE) in the promoter region of target genes. The active conformation of the VDR forms a surface called the activation function 2 (AF-2) to which coactivator complexes are recruited, and this triggers complex events that lead to transactivation.[4]

Mutations in the VDR gene cause the genetic diseases hereditary vitamin D-resistant rickets (HVDRR, also known as vitamin D-dependent rickets, type II).[7] HVDRR, an autosomal recessive disorder, is characterized by early onset rickets, hypocalcemia, elevated serum $1,25(OH)_2D_3$ level, and secondary hyperparathyroidism. Mutations are found in both the DNA binding domain (DBD) and ligand binding domain (LBD) of the VDR. One major therapeutic approach to HVDRR is the intravenous injection of calcium;[7b] however, this treatment must be continued for a long period and fails to improve patients' quality-of-life. Therefore, other therapeutic options are needed. For example, small compounds might

Received: April 14, 2013
Published: August 14, 2013

   dx.doi.org/10.1021/jm400537h | J. Med. Chem. 2013, 56, 6745−6760

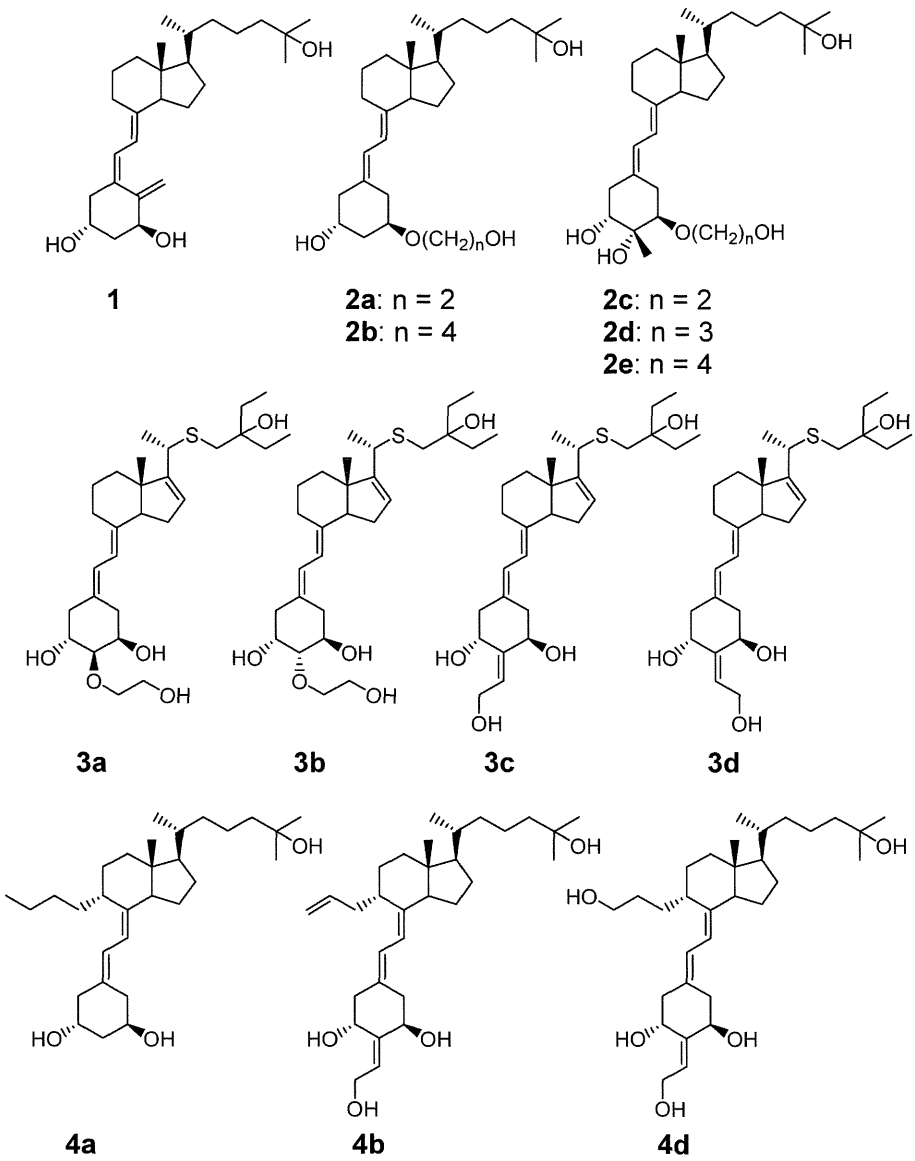

Figure 1. Structures of the vitamin D analogues discussed in this article.

rescue the functions disrupted by the missense mutations in the VDR-LBD.

Fifteen missense mutations have been identified in the LBD[7b] that reduce or abolish VDR functions, such as ligand binding and ligand-dependent transactivation. So far, only the crystal structure of the HVDRR H305Q mutant has been reported.[8] The H305Q mutation causes a 10-fold reduction in $1,25(OH)_2D_3$-dependent transactivation, and patients with this mutation can be treated with the natural hormone. The missense mutation R274L,[9] however, causes a >1000-fold reduction in responsiveness to the natural hormone. Patients with this mutation are hardly responsive to treatment with $1,25(OH)_2D_3$. Another severe mutation is W286R.[10] Patients with this mutation never respond to the natural hormone.

Here, we present the crystal structures of rat (r) VDR-LBD R270L and W282R mutants, which correspond to the human (h) R274L and W286R VDR mutants, respectively. We also designed and synthesized several ligands (**2a–e**, **3a–d**, and **4a–e**) (Figure 1) for use with these mutants. On the basis of these crystal structures and results of in vitro biological assays with ligands (**2a–e**, **3a–d** and **4a–e**), we discuss how these mutations disrupt the VDR function. Our data also provide clues for the design of novel therapeutic compounds for the treatment of HVDRR patients. Thermal unfolding experiments and CD spectral analysis also provided data that could not be obtained from the X-ray analysis alone to characterize these mutants.

RESULTS

Crystal Structures. We crystallized the rat VDR-LBD with a deletion mutation (rVDR-LBD 116–423, Δ165–211) in the long loop between helices H2 and H3[11] because it readily provided high quality crystals even with the point mutations. Human and rat VDRs share 89.5% identity overall and are 97.2% identical within the ligand-binding pocket (LBP). Therefore, crystal structures of rVDR-LBD mutants also provide important structural information about hVDR-LBD mutants. From this point in this article, rVDR-LBD (Δ165–211) will be referred to as WT, and its substitution mutants will be referred to as R270L and W282R, respectively.

The crystals of WT, R270L, and W282R were grown in the presence of the natural hormone (**1**) or one of the ligands

dx.doi.org/10.1021/jm400537h | J. Med. Chem. 2013, 56, 6745–6760

designed for the mutants (**3c** and **3d** for R270L, **4a** and **4b** for W282R; Figure 1) and with a peptide containing the LXXLL motif derived from the coactivator DRIP205 (MED1).[12] This peptide, which is essential for crystallizations, not only stabilizes the crystals by binding to the surface between the termini of the helices H3 and H12, known as the coactivator recognition surface (the AF-2 surface), but also participates in crystal packing (Figure S1, Supporting Information).

All of the crystals belonged to the same space group *C*2 as other rVDR complexes do.[11,13] The R270L complexes with ligands **1**, **3c**, and **3d** were refined to resolutions of 1.70, 1.90, and 2.11 Å (PDB ID: 3VT3, 3VT4, and 3VT5, respectively). The WT complex with ligand **3c** was refined to a resolution of 2.30 Å (PDB ID: 3VT6). The W282R complexes with ligands **1**, **4a**, and **4b** were refined to resolutions of 1.65, 2.10, and 2.35 Å (PDB ID: 3VT7, 3VT8, and 3VT9, respectively). Summaries of data collection and refinement statistics are shown in Tables S1, S2, and S3 (Supporting Information).

The overall folds of the VDR-LBDs in these complexes were fundamentally identical to those of the known h- and rVDR-LBD complexes with the natural hormone,[11a,14] as well as its agonistic[13c,15] and antagonistic analogues.[11b,13a,b,d] All seven complexes adopted the canonical active conformation of the VDR-LBD, and the coactivator peptide bound to the AF-2 surface. The root-mean-square deviations (rmsd) of the equivalent Cα atoms of the mutants (R270L and W282R) complexed with 1,25$(OH)_2D_3$ and the synthetic ligands (**3c**, **3d**, **4a**, and **4b**) from the corresponding WT complex (PDB ID: 2ZLC) were 0.15 to 0.30 Å. For comparison, we used rVDR-LBD (2ZLC) reported by us[16] but not that (1RK3) reported by Vanhooke's group[11a] because the conditions we used to prepare the crystals were nearly identical to those used for 2ZLC. The difference in the crystallization conditions used caused some changes in the loop region structures (rmsd, 0.4–0.9 Å). In calculating Cα rmsds, we eliminated the terminal atoms that had large rmsds values of >1.00.

R270L Complexed with the Natural Hormone 1,25-$(OH)_2D_3$. We successfully crystallized R270L complexed with 1,25$(OH)_2D_3$ in its active ternary complex as evidenced by the corresponding density clearly seen in the $2F_{obs} - F_{calc}$ map (Figure S2, Supporting Information). The Cα structure was nearly identical to that of WT (2ZLC), as indicated by the total rmsd (0.15 Å). The Cα positions shifted slightly near the mutation, Leu269 (0.45 Å) and Met268 (0.30 Å). Two water molecules are found in the space created by the mutation of arginine to leucine (Figure 2A); one of these water molecules forms a hydrogen bond with the 1α-OH group, and the other forms a hydrogen bond with the main chain carbonyl group of Thr142. These interactions, however, must be weak because the human R274L mutant showed a greater than 1000-fold reduction in transcriptional responsiveness to the natural hormone.[9] In the WT, Arg270 formed direct hydrogen bonds with the 1α-OH group and the main chain carbonyl of Thr142. These direct interactions might be important to keep the conformation of the loop 1–2 and for the function of the VDR. Ligand recognition by the mutant, otherwise, is very similar to that of the WT, that is, 1,25$(OH)_2D_3$ (**1**) is anchored by five hydrogen bonds.

R270L in Complex with Ligands 3c and 3d. Ligands **3c** and **3d** are super agonists for wild-type hVDR.[16] They were also good agonists for R274L hVDR, being 130 and 40 times, respectively, more potent than **1** (see below). The complexes of R270L with **3c** and **3d** adopt the same active conformation as

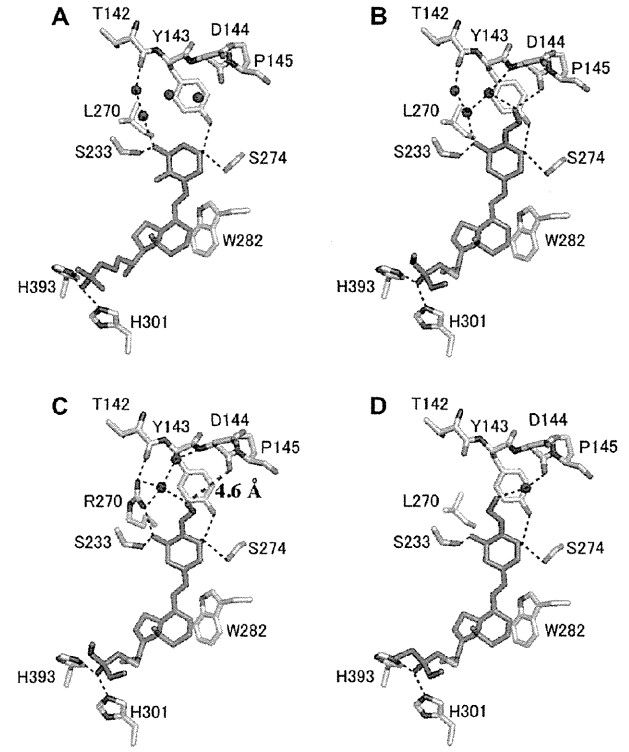

Figure 2. Hydrogen-bonding interactions in the complexes of R270L. (A) R270L with **1**, (B) R270L with **3c**, (C) WT with **3c**, and (D) R270L with **3d**. Black dotted lines show hydrogen bonds. Ligands (dark gray, carbon; red, oxygen; and yellow, sulfur) and protein residues (white, carbon; red, oxygen; and blue, nitrogen) are shown as sticks and water molecules as red balls. The magenta dotted line in C shows the distance between the terminal hydroxyl group of **3c** and the main chain carbonyl group of Asp144.

that of the WT. The Cα rmsds of R270L complexed with **3c** and **3d** from WT (2ZLC) were 0.23 and 0.19 Å, respectively.

In the complex of R270L with **3c**, the terminal hydroxyl group of the substituent at C(2) directly interacts with the main chain carbonyl group of Asp144 (Figure 2B). This interaction replaced the lost direct interactions among the 1α-OH group of the ligand, Arg270, and Thr142 and explain why **3c** was 130 times more active than **1** for hR274L. The defective interaction with L270 made the ligand slightly move to Asp144 to form the hydrogen bond. In the complex with WT (Figure 2C), the terminal hydroxyl group of **3c** was 4.6 Å away from the carbonyl group of Asp144. Compound **3c** also interacted with Thr142 via two water molecules (Figure 2B). Because of these interactions, the Cα positional shifts of Thr142, Asp144, and Pro145 from those of the WT/1,25$(OH)_2D_3$ complex were somewhat large at 0.40, 0.55, and 0.63 Å, respectively. These changes might affect the conformation of Gln273 (positional shift, 0.48 Å) and Ser274 (0.48 Å) in the H5. Other than this difference, **3c**'s interaction with R270L was essentially identical to that with WT.

In the complex with R270L, **3d** does not directly hydrogen bond with Asp144, but it does hydrogen bond with a water molecule that, in turn, interacted with Asp144 (Figure 2D). This difference explains the difference in the activity of **3d** compared with **3c**.

W282R with Several Ligands. Trp286 in the hVDR-LBD (Trp282 in rVDR-LBD) interacts strongly with the vitamin D ligand.[11a,14] The interactions occur at its 2-, 3a-, 4-, and 7a-

dx.doi.org/10.1021/jm400537h | J. Med. Chem. 2013, 56, 6745–6760

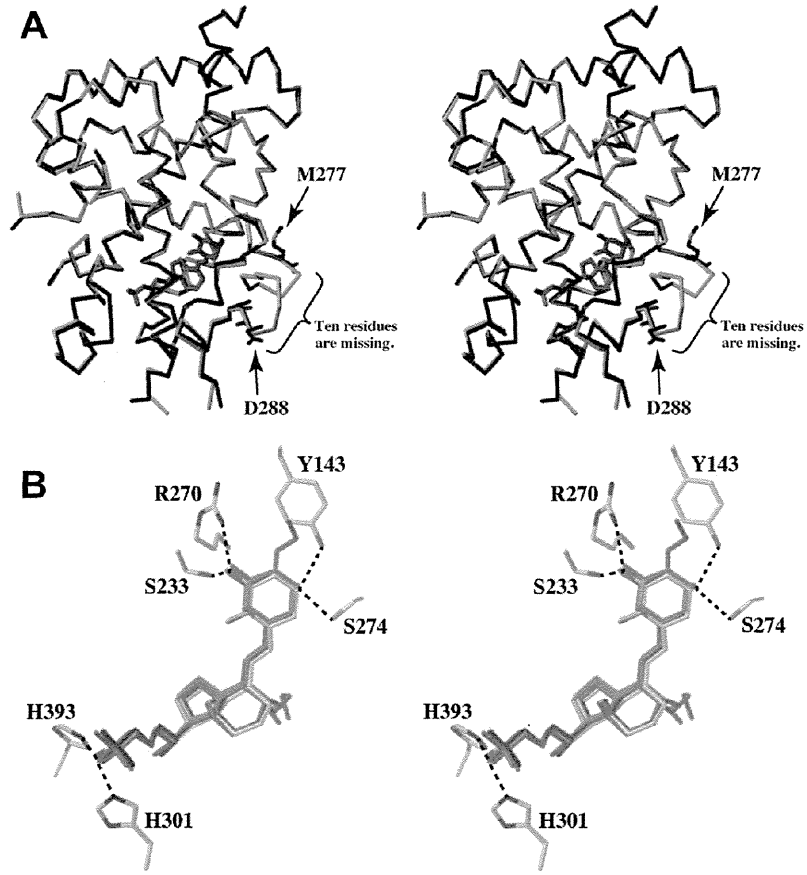

Figure 3. Overlays of the crystal structures of W282R and WT (stereoviews). (A) Overlay of the Cα structures of W282R and WT in complex with 1,25$(OH)_2D_3$ (WT, yellow protein with green ligand; W282R, blue protein with magenta ligand). The W282R structure lacks 10 residues from Asp278 to Gln287. (B) Overlay of the ligands in WT (2ZLC) (atom type) and in W282R (**1**, **4a**, and **4b**; blue, green, and magenta, respectively) and the hydrogen-bonding residues in 2ZLC. The dotted lines show hydrogen bonds.

positions with the 6-, 8-, and 9-positions of the ligand over distances of less than 4 Å (Figure S3A, Supporting Information). The Trp286 also interacts with Phe279, Gln317, Tyr295, Ser275, Ser278, Leu313, and Ile314. As a result, its mutation to Arg abolishes the activity of the VDR mutant.[10]

We succeessfully crystallized ternary complexes of the W282R mutant with the natural hormone and two synthetic ligands (**4a** and **4b**), and the coactivator-derived peptide. The 9α-substituted ligands (**4a** and **4b**) were designed on the basis of the model of the mutants. The substituent at the 9α-position was directed toward Trp282 and expected to occupy the space yielded by the Trp to Arg mutation (Figures S3B and S4C, Supporting Information).

W282R in Complex with the Natural Hormone. The crystal structure of W282R in complex with the natural hormone was determined as the canonical active conformation (Figure 3A). Surprisingly, a group of residues neighboring of Arg282 were not visible in the electron density map of the mutant complex with the natural hormone (Figures 4A and B), suggesting that these residues were highly disordered. We did not observe any interpretable density in the W282R structure for 10 residues between Asp278 and Gln287 (Figure 4A). This disorder at the β-strand part affected the conformation of the beginning of loop 1–2, from Pro145 to Ala148 (positional shift, 0.35–0.79 Å). Yet, despite such a drastic disorder in the secondary structure, the overall folds of the mutant remain nearly identical to those of the WT (rmsd 0.27 Å) (Figure 3A). We assume that the coactivator peptide trapped the active conformation of the mutant by binding to the AF-2 surface, which formed temporally when the mutant bound the ligand. Thus, the seemingly minor conformation of W282R in biological solutions was crystallized out under our crystallization conditions. Surprisingly, the ligand forms normal hydrogen bonds via its three hydroxyl groups (Figure 3B).

W282R with 9-Substitued Vitamin D Analogues (4a and 4b). The complexes of W282R with **4a** and **4b** exhibited similar disorder near the antiparallel β-sheet; the seven residues from Asp279 to Gly285 were not visible. In addition, the ligands themselves had high temperature factors at the terminal of the 9-substituent groups. For example, in the complex of W282R with **4a** or **4b**, the terminal atom of the 9-substituent had an especially high value of more than 45 $Å^2$ (Figures S3C and D, Supporting Information). Thus, the terminal atoms of the 9-substituents cannot be stabilized via interactions to receptor residues that are also disordered. However, both **4a** and **4b** form normal hydrogen bonds via their three hydroxyl groups (Figure 3B).

Ligand Additive Effects and Thermal Unfolding of rVDR-LBD Mutants Observed by Far-UV CD Spectra. To examine the thermal stability of the R270L and W282R mutants compared with WT, we monitored heat-induced unfolding transition experiments using CD spectra.[17] Equilibrium CD spectra were obtained in the far-UV regions at pH 7.0. The far-UV spectrum of a solution of ligand-free WT at 20 °C exhibited the typical spectrum of an α-helical structure, and

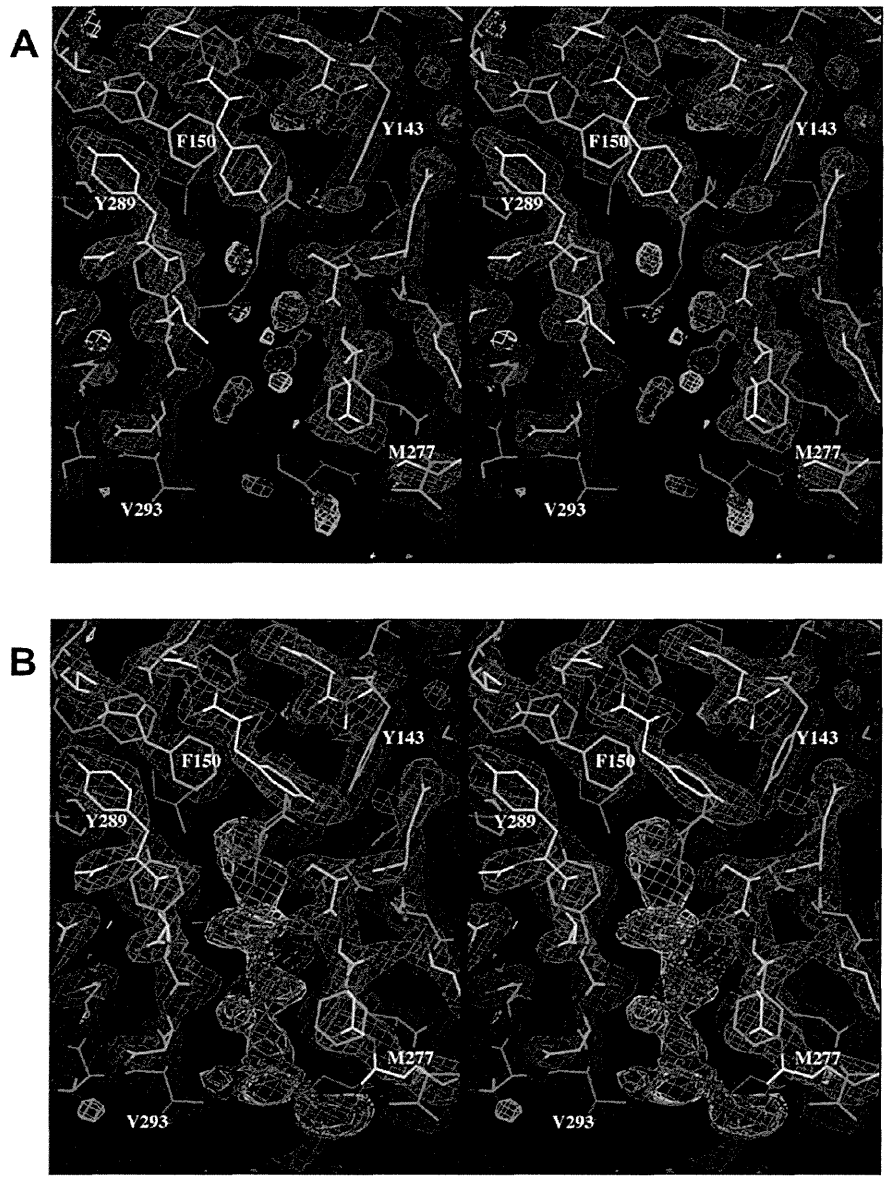

Figure 4. Electron density maps of W282R and WT complexes. (A) Electron density map of W282R/1,25$(OH)_2D_3$ around the β-sheet region (stereo view). (B) Electron density map of WT/1,25$(OH)_2D_3$ (PDB ID: 2ZLC) in the same region and orientation as that described above (stereo view). The $2F_{obs} - F_{calc}$ map (1.5 σ) is shown in blue, and the $F_{obs} - F_{calc}$ map (3 σ) is shown in pink. Notice that electron density around R282 (from Asp278 to Gln287) is missing in A but not in B.

the addition of the natural hormone confirmed this α-helical type spectrum[18] (Figure S5A, Supporting Information). R270L and W282R showed similar α-helical spectra to that of WT including the ligand-additive effect (Figures S5B and C, Supporting Information).

However, the three proteins WT, R270L, and W282R showed remarkable differences in their thermal stability. Figure S5D, E, and F (Supporting Information) shows the equilibrium transition curves at 222 nm of WT, R270L, and W282R, respectively, with and without the natural hormone. In the ligand-free solutions, the transition temperature (T_m) of WT was the highest (47.8 °C), whereas those of R270L and W282R were similarly lower (44.1 and 44.8 °C, respectively). In the presence of the natural ligand, the differences in the T_m values were more distinct. Ligand binding caused the T_m of WT to rise by 8.4 °C, whereas the T_m of R270L and W282R rose by only 2.5 and 0.1 °C, respectively. These results indicate that the ligand significantly stabilizes the WT but only weakly stabilizes R270L and has no stabilization effect on W282R. These results are consistent with the ligand binding behavior of the three proteins.

Synthesis of Agonists for Mutants R274L and W286R.

Agonist for R274L. Several studies have been reported to create specific agonist for mutants implicated in HVDRR. Swann et al.[19] reported that nonsecosteroidal ligands with a bisphenol scaffold showed potent transactivation for R274L. Kittaka et al. reported that vitamin D_3 analogues modified at the 1α-, 1β-, or 2α-position on the A-ring of vitamin D_3 improved the vitamin D action on the R274A and R274L mutants.[20]

We also designed and synthesized candidates of **2a–2e** and **3a–d** for hR274L (rR270L) (Figure 1). These candidates are 19-norvitamin D_3 analogues modified at the 1α-position (**2a** and **2b**), 1α- and 2-positions (**2c–2e**), and the side chain and 2-position (**3a–3d**).[16] Computer-aided molecular modeling

dx.doi.org/10.1021/jm400537h | J. Med. Chem. 2013, 56, 6745–6760

Scheme 1. Synthesis of Ligands 2a and 2b

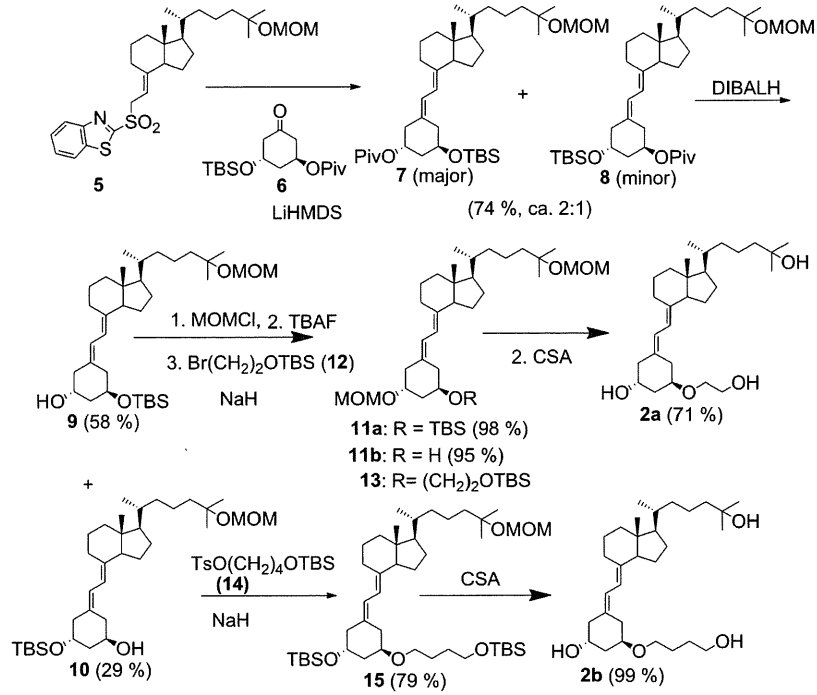

Scheme 2. Synthesis of Ligands 2c to 2e

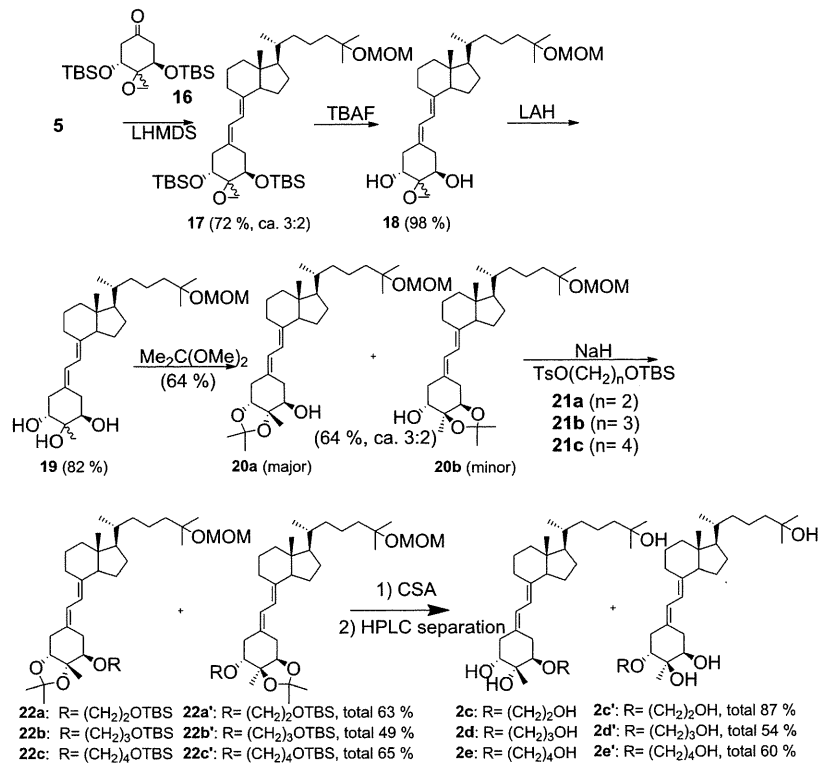

(Sybyl, Tripos) was used to design these ligands. The long substituent at the 1α-position was designed to fill the space newly generated by the Arg to Leu mutation (Figure S4A, Supporting Information). The 2α-methyl group of **2c**–**2e** was expected to interact with the hydrophobic residue above the A-ring and the 2β-hydroxyl group with the polar environment below the A ring.

The synthetic scheme of **2a** and **2b** is shown in Scheme 1. Julia-Kocienski reagent **5**[21] was coupled with A-ring fragment **6**, in which 1α- and 3β-hydroxyl groups were distinguished by protecting groups, to give 19-norvitamin D **7** and **8** as a 2:1 mixture (74%). After the pivaloyl group was removed (DIBALH), the free hydroxyl group of **9** was protected with the methoxymethyl (MOM) group (98%), and the *t*-butyldimethylsilyl (TBS) group was deprotected (95%) and

dx.doi.org/10.1021/jm400537h | J. Med. Chem. 2013, 56, 6745–6760

Scheme 3. Synthesis of Ligands 4a–4e

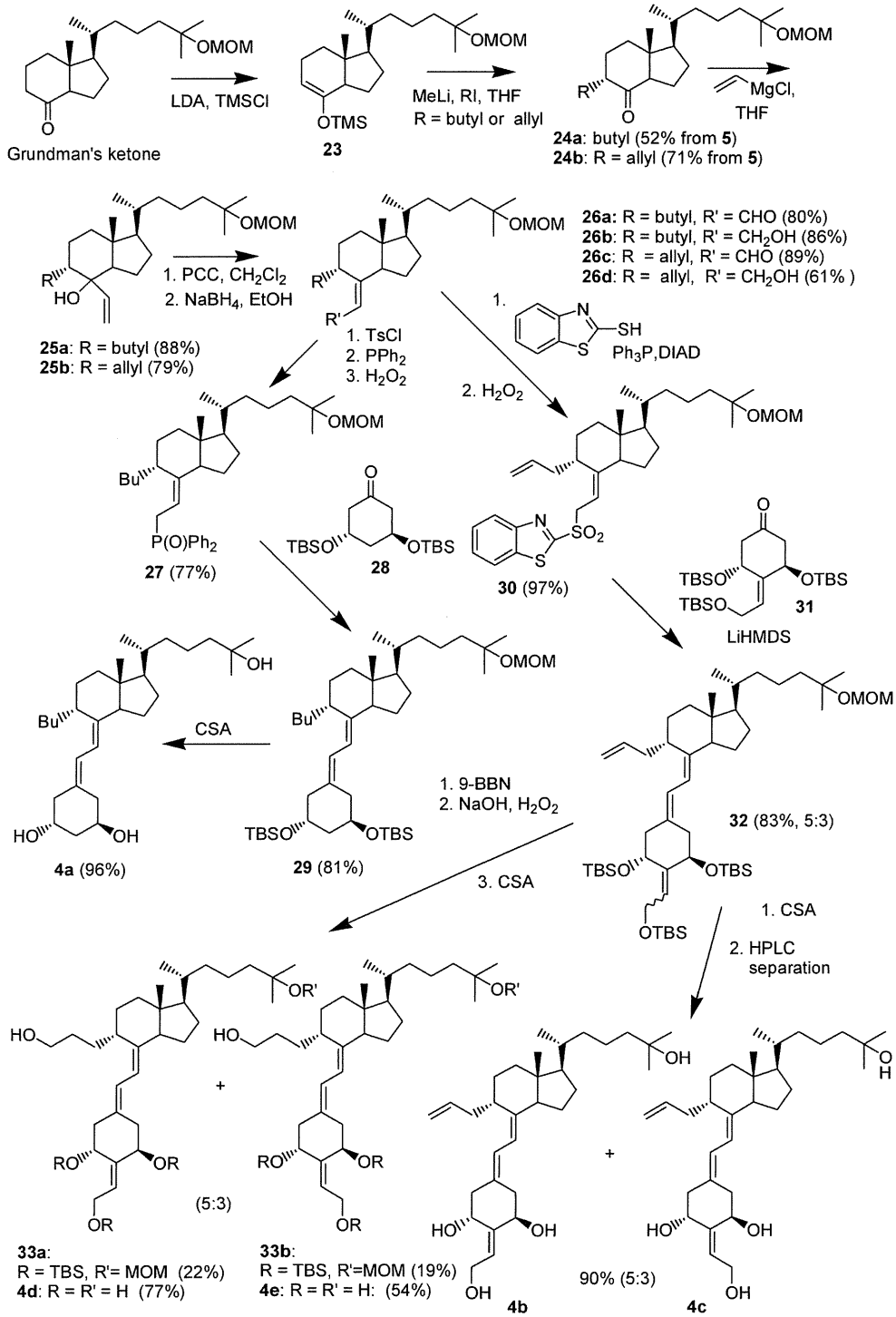

then treated with bromide **12** to give **13** (23%), the protecting groups of which were removed with camphor sulfonic acid (CSA) in MeOH to give 1α-hydroxyethoxy compound **2a** (71%). The hydroxy group of **10** was treated with tosylate **14** to give **15** (79%), the protecting groups of which were removed with CSA to give **2b** (99%).

The analogues **2c–e** were synthesized from **5** (Scheme 2). Compound **5** was treated with A-ring fragment **16** (72%), the TBS group was removed (98%), and the epoxide group was reduced with LAH to give triol **19** as an epimeric mixture at C(2) (82%). The *cis*-vicinal hydroxyl group of **19** was protected with 2,2-dimethoxypropane to give a 3:2 mixture of 2,3 (**20a**)- and 1,2-ketals (**20b**) (64%), and the remaining hydroxyl group was treated with tosylates **21a**, **21b**, and **21c** to give **22a**, **22b**, and **22c** (63%, 49%, and 65%), respectively. The protecting groups were removed with CSA, and then the products were separated by HPLC to give **2c**, **2d**, and **2e** and their regioisomers (total 87%, 54%, and 60%, respectively). The synthesis of **3a–d** was reported previously.[16]

Agonist for W286R. Using models of the W282R mutant, we hypothesized that a larger butyl group added to replace the 9α-hydrogen of vitamin D (Figure S3B, Supporting Information)

dx.doi.org/10.1021/jm400537h | J. Med. Chem. 2013, 56, 6745–6760

would fill the space formed upon substitution of the Trp to Arg (Figure S4C, Supporting Information). Thus, we synthesized vitamin D compounds substituted with a butyl (**4a**), allyl (**4b**), or 3-hydroxypropyl (**4d**) group at the 9α-position (Scheme 3).

Grundman's ketone was converted to enol trimethylsilyl ether (**23**), which was treated in situ with MeLi followed by butyl iodide or allyl iodide to give the 9α-substituted ketones **24a** or **24b** (71% or 52%, respectively). The ketones (**24a** and **24b**) were treated with vinyl magnesium chloride (**25a** 88% and **25b** 79%, respectively), oxidized with PCC to give aldehydes **26a** (80%) and **26c** (89%), respectively, which were then reduced to give alcohols **26b** (86%) and **26d** (61%), respectively. Compound **26b** was converted to Wittig reagent **27** (77%), combined with A-ring fragment **28** (21%, 74% based on the recovery of the starting material **27**), and deprotected with CSA to give **4a** (96%). The low yield of the Wittig–Horner reaction was probably due to the steric inhibition of the 9α-butyl group. For the synthesis of **4b–e**, we employed the Julia-Kociensky reaction to couple the A-ring and CD-ring fragments. Allyl alcohol **26d** was treated with 2-mercaptobenzothiazole in the presence of triphenyl phosphine and DIAD and then oxidized with H_2O_2 to give **30** (97%). Compound **30** was treated with A-ring fragment **31** to give **32** (57%, 83%, on the basis of the recovered **30**) as a 5:3 mixture of *E*- and *Z*-isomers at C(2), which were deprotected and separated by HPLC to give **4b** (2*E*-isomer) and **4c** (2*Z*-isomer) (5:3, 90% total). To obtain 9-hydroxypropyl compounds, **32** was allowed to undergo hydroboration followed by oxidation and deprotection to give **4d** (17% in three steps, 2*E*-isomer) and **4e** (10% in three steps, 2*Z*-isomer).

Biological Evaluation of Synthetic Ligands. *Ligands for R274L.* Ligands **2a** and **2b** were less active than the natural hormone in the luciferase assay with hR274L, and ligands **2c–e** have almost no potency (Figure 5A). Molecular modeling predicted a space that would be generated in the LBP by the mutation of Arg270 to Leu (Figure S4A, Supporting Information). However, the actual space in the LBP of R270L crystal structure differed slightly from the predicted space (Figure S4B, Supporting Information). The R270L had a pocket (Figure S4B, Supporting Information, yellow) that was narrower than we expected on the basis of the model (Figure S4B, Supporting Information, green), and accordingly, ligand **2b** did not fit correctly in the LBP of R270L. This difference was likely due to a slight movement of helix H5, which is difficult to predict by modeling. Therefore, the 1α-substituents of ligands **2a–e** were unable to enter the LBP due to steric congestion.

The ligands (**3a–3d**), which were initially designed as super agonists,[16] showed excellent activity for R274L: **3a**, **3b**, **3c**, and **3d** were 15, 4, 130, and 46 times more potent than **1** for R274L in transactivation (Figure 5B). Interestingly, while 2β-hydroxyethoxy-D analogue (**3b**) was the most potent for the WT VDR,[16] the 2*E*-hydroxyethylidene analogue (**3c**) appeared to be the most potent for the R274L mutant. Ligand **3c** had the highest activity for R274L because its terminal hydroxyl group directly interacted with the main chain carbonyl group of Asp144 (Figure 2B). Thus, **3c** may be a good candidate for the treatment of HVDRR caused by the R274L mutation.

Ligand **3d** was less active than **3c** for R274L because it interacted with Asp144 via a water molecule (Figure 2D). These results indicate that direct interactions are much stronger than indirect interactions via water.

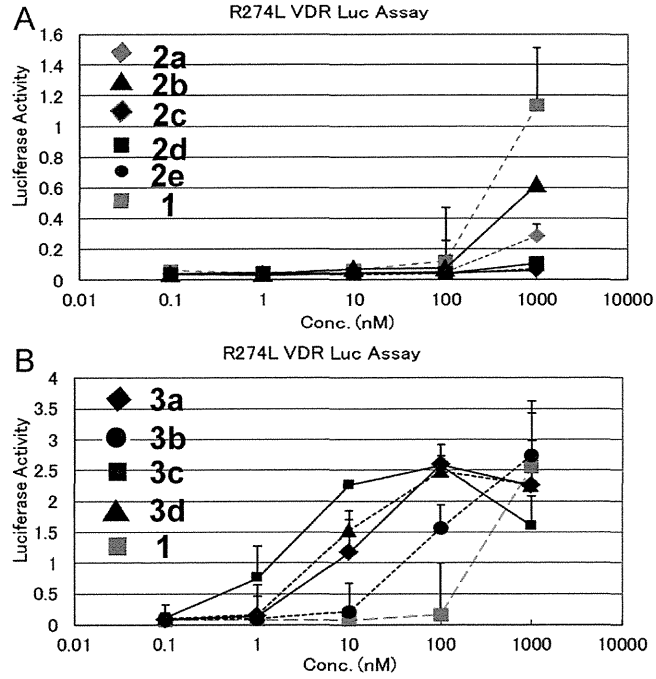

Figure 5. Transcriptional activities of **1** and synthetic ligands on R274L hVDR. The activities of **2a–e** and **1** (A) and **3a–d** and **1** (B) were evaluated by dual luciferase assay using a R274L full-length hVDR expression plasmid (pCMX-hVDR) and a luciferase reporter gene with a mouse osteopontin VDRE at the promoter (SPPx3-TK-Luc) in COS7 cells.

Ligands for W286R. Despite our design (Figures S3B and S4C, Supporting Information) and efforts, the 9-substitued compounds we synthesized had little to no potency on W286R hVDR (**4a** and **4c** to **4e**, data not shown; **4b**, see Figure S6, Supporting Information). The hydrophobic 9-substituent groups did not induce better folding of the disordered β-strands. The temperature factors shown on the ligand (Figure S3C and D, Supporting Information) suggest that shorter substituents would be better. Our findings also suggest that a negatively charged group introduced at the 9α-position may hold the Arg282 side chain inside the LBP, thereby maintaining the normal folding of the β-sheet part.

DISCUSSION

Structures of the R270L and W282R Mutant Proteins Would Be Trapped under Our Crystallization Conditions and Represent a Minor Population in Biological Solutions. Regardless of the mutants' low potency, the crystal structures of the ternary complexes of the mutant rVDRs adopted canonical active conformations. Because of the importance of the DRIP205 peptide in crystallization, it is clear that the peptide trapped the ligand-bound active conformation. Packing modes in the unit cell also supported crystallization of the active conformation (Figure S1, Supporting Information). In the most N-terminal part of the R270L complexed with the natural hormone (**1**), electron density of the residues of the expression tag sequence (Asn-Ser-Pro) was observed (Figure S1A and C, Supporting Information, red helix). These residues interact with Asp137 and His140 in the neighboring molecule in the crystal (Figure S1C, Supporting Information). In the crystal of W282R, the interactions of His130 with Glu304 and Glu307, and of Arg248 with Glu392 in the neighboring molecule were also

observed (Figure S1E, Supporting Information). These interactions between neighboring molecules were not observed in WT rVDR-LBD.

In contrast, thermal transition experiments in the solution state using CD spectra indicated that R270L was present in a nearly ligand-free and W282R completely ligand-free states, whereas WT was completely in the ligand-bound state. From all of these results, we concluded that these mutants R270L and W282R were crystallized as the complexes with ligands in the active conformations probably because the coactivator peptide binds to the AF-2 surface thereby stabilizing the complex. It is also clear that these mutants are free of the ligands in biological solution, as supported by the CD spectral analysis and by their biological activities.[9,10]

Substitution Mutation R270L Causes a Significant Change in the Main Chain Structure between Helices H1 and H2. The substitution mutation led to a local conformational change in the protein structure. A small difference (rmsd 0.13−0.28) in the coordinates of R270L/1,25$(OH)_2D_3$ compared with those of WT/1,25$(OH)_2D_3$ would be important. Arg274 in hVDR is essential for its interaction with the 1α-OH group of the ligand.[22] However, Arg274 also has an important interaction with the main chain carbonyl group of Thr142. The loop 1−2 of agonist-bound VDR-LBDs derived from humans, rats, and zebra fish, shares common secondary structural characteristics:[11a,14,15d] Glu126 to Thr142 displays a typical α-helix (H1), Thr142 to Pro145 forms a β-strand-like structure, Pro145 and Thr146 form a hydrogen-bonded turn, and Ala148 to Asp152 displays a 3_{10}-helix (H2). Thr142 and Tyr143 are particularly notable because they are tethered to the natural hormone. The Tyr143 side chain interacts directly with the 3β-OH of the ligand, and the Thr142 main chain carbonyl group interacts with Arg270, which interacts with the 1α-OH of the ligand. In the R270L mutant, Thr142 and 1α-OH are connected by interactions via two water molecules. Thus, one of the two interactions is weakened by the mutation. We previously performed a mutational analysis of all of the LBP residues of the VDR and reported that the single mutation of Y143A causes a marked reduction in ligand-dependent transactivation.[22,23] These results suggested that the local area structures between H1 and H2 influence ligand-dependent VDR functions. We confirmed in the present studies that water-mediated interactions are weaker than direct interactions between ligands and residues.

In the present study, the 2-substituted-19-norvitamin D_3 analogues **3a**, **3b**, **3c**, and **3d** showed potent agonistic activity against the hVDR R274L mutant (Figure 5B). Of these four derivatives, **3c** was the most effective agonist against the R274L mutant, whereas **3b** was the most effective against the WT VDR. We, therefore, suggest that **3c** is the most promising candidate among these analogues for the treatment of HVDRR caused by the R274L mutation.

Why Does the W286R Mutant Never Respond to Vitamin D Ligands? We also obtained the crystal structures of the W282R mutant as the ligand-bound active conformation. These structures would also represent a minor population in a biological solution because previous studies have shown that W286R hVDR never binds to the natural hormone and never responds to vitamin D-dependent gene transactivation.[10] However, the structures of these complexes have a notable feature. Ten to seven residues around the mutated part of the protein complexed with either 1,25$(OH)_2D_3$ or ligand **3a** or **3b** were not visible. Every VDR-LBD, including those of rats, humans, and zebra fish, has a set of antiparallel β-sheets. From the center of the β-sheet, Trp282 (or Trp286 in hVDR) protrudes to the seco-B and C ring parts of the ligand, where they strongly interact (Figure S3A, Supporting Information). In general, proteins favor hydrophobic residues on the inside and hydrophilic residues on the outside. Thus, unlike Trp, the hydrophilic Arg282 would favor the outside rather than the inside. This disruption of the β-strand conformation could lead to a partial unfolding of this part of the complex. We conclude that correct folding at the β-strand part is important for the VDR action. It has been reported[24] in the crystal structural study of intact peroxisome proliferator activating receptor γ (PPARγ)-RXRα complex on DNA that the β-sheet parts of the PPARγ form hydrophobic interactions with RXRα DBD and that these interactions can contribute to DNA recognition and affinity. The β-sheet part of the VDR may have similar function. A CD spectral study showed the stabilities of the WT, and the mutant widened drastically when the ligand was present. The mutation spoils the stability gain of the VDR upon ligand binding.

We designed the agonists (**4a**, **4b**, and **4d**) for the W286R mutant by paying attention to the position (C-9) of modification in the ligand. In future studies, we plan to examine the electronic compatibility of the ligand with the Arg side chain. For example, it would be interesting to introduce a negatively charged group at the 9α-position of the ligand.

CONCLUSIONS

We solved the crystal structures of two rVDR-LBD mutants implicated in HVDRR, R270L, and W282R, complexed with natural and synthetic vitamin D ligands and the coactivator DRIP205 peptide. All of the crystal structures adopted canonical active conformations. However, these active conformations are assumed to be minor conformations in biological solutions because the responsiveness of these mutants to the natural hormone are severely reduced or even eliminated. The binding of the coactivator peptide to the AF-2 surface may have facilitated the crystallization of the complex.

The mutations caused only local conformational changes. In R270L, we observed small Cα rmsd changes in the residues near the R270L mutation and the loss of direct interactions of Arg270 with the ligand and with Thr142. The hydroxyethylidene side chain at C(2) of analogue **3c** formed a hydrogen bond with Asp144 and restored the potency that was reduced by the mutation. We suggest that **3c** has potential as an agent for the treatment of HVDRR caused by the R274L mutation.

The W282R mutation disrupted the structure around the β-strands so that 7 to 10 residues around that position became invisible. This occurred probably because the Trp to Arg mutation changed the property of this portion from hydrophobic to hydrophilic. However, it should be noted that in the W282R/ligand complexes, all three hydroxyl groups of the ligands (**1**, **4a**, and **4b**) were doubly anchored by a pair of hydrogen bonds to the protein residues, suggesting that the six hydrogen bonds are not enough for the VDR in biological solution to anchor the ligands. Maintenance of the conformation around the β-strands is important for VDR function. We, therefore, suggest that vitamin D derivatives with a 9α-substituent that has a negative charge may be suitable agents to keep the arginine side chain inside the LBP to activate W286R.

dx.doi.org/10.1021/jm400537h | J. Med. Chem. 2013, 56, 6745−6760

EXPERIMENTAL PROCEDURES

Protein Expression and Purification. To obtain the mutant VDR-LBD genes, we used QuikChange Site-Directed Mutagenesis Kit (Stratagene) and performed PCR with pET14b/rVDR-LBD plasmid[11b] as a template.

The rat VDR-LBDs (residues116–423 and Δ165–211) with or without the mutations were cloned as an N-terminal His6-tagged fusion protein into the pET14b expression vector and overexpressed in *Escherichia coli* C41, which is a modified strain from BL21. The cells were grown at 37 °C in LB medium (including ampicilin-Na 100 mg/L) and subsequently induced for 6 h with 15 μM isopropyl-β-D-thiogalactopyranoside (IPTG) at 23 °C. The purification procedure included affinity chromatography on a Ni-NTA column, followed by dialysis and ion-exchange chromatography (SP-sepharose). After tag removal by thrombin digestion, protease was removed by filtration through a HiTrap benzamidine column, and the protein was further purified by gel filtration on a Superdex200 column. The purity and homogeneity of the rVDR-LBD were assessed by SDS–PAGE.

Crystallization. Crystallization conditions for WT, R270L, and W282R have some difference. Purified WT solution was concentrated to about 0.75 mg/mL by ultrafiltration. To an aliquot (800 μL) of the protein solution was added each ligand (ca. 10 equivalents), the solution was further concentrated to attain about 100 μL, and then a solution (25 mM Tris-HCl, pH 8.0; 50 mM NaCl; 10 mM DTT; and 0.02% NaN_3) of coactivator peptide (H_2N-KNHPMLMNLLKDN-$CONH_2$, ca. 5 equivalents) derived from DRIP205 was added. These solutions of WT/ligands/peptide were allowed to crystallize by the vapor diffusion method using a series of precipitant solutions containing 0.1 M MOPS-NaOH (pH 7.0), 0.1–0.4 M sodium formate, 12–22% (w/v) PEG4000, and 5% (v/v) ethylene glycol.

Purified R270L solution was also concentrated to about 0.75 mg/mL by ultrafiltration. To an aliquot (800 μL) of the protein solution was added each ligand (ca. 10 or 20 equivalents), the solution was further concentrated to attain about 100 μL, and then the peptide solution was added. These solutions of R270L/ligands/peptide were allowed to crystallize using a series of precipitant solutions containing 0.1 M MOPS-NaOH (pH 7.0) (or 0.1 M Tris-HCl (pH 8.0), or 0.1 M glycine-NaOH (pH 9.0)), 0.4 M sodium formate, and 12–22% (w/v) PEG4000.

Purified W282R solution was concentrated to about 1.7 mg/mL by ultrafiltration. To an aliquot (350 μL) of the protein solution was added each ligand (ca. 10 or 20 equivalents), the solution was further concentrated to attain about 100 μL, and then the peptide solution was added. Solutions of W282R/natural hormone (**1**) or ligand **4a**/peptide were allowed to crystallize using a series of precipitant solutions containing 0.1 M MOPS-NaOH (pH 7.0), 0.05–0.2 M diammonium citrate, 14–26% (w/v) PEG4000, and 4% (v/v) 2-propanol. The other solution of W282R/ligand **4b**/peptide was allowed to crystallize using a series of precipitant solutions containing 0.1 M MOPS-NaOH (pH 7.0), 0.1 M sodium formate, 18–22% (w/v) PEG4000, and 5%(v/v) ethylene glycol.

Droplets for the crystallizations were prepared by mixing 2 μL of complex solution and 1 μL of precipitant solution, and droplets were equilibrated against 500 μL of precipitant solution at 20 °C. It took 1 to 3 days to obtain crystals with X-ray diffraction quality. The peptide derived from DRIP205 was essential for all of our crystallizations.

Diffraction Experiment and Structure Analysis. Prior to diffraction data collection, crystals were soaked in cryoprotectant solutions containing 17–20% ethylene glycol and the other reagents. Diffraction data sets were collected at 100 K in a stream of nitrogen gas at beamline BL-6A of KEK-PF and NW12A of PF-AR (Tsukuba, Japan). Reflections were recorded with an oscillation range per image of 1.0°. Diffraction data were indexed, integrated, and scaled using the program HKL2000.[25] The structures of complexes were solved by molecular replacement with the program CNS,[26] and finalized sets of atomic coordinates were obtained after iterative rounds of model modification with the program XtalView[27] and refinement with CNS by rigid body refinement, simulated annealing, positional minimization, water molecule identification, and individual isotropic B-value refinement.

Thermal Unfolding Measurement. Circular dichloism (CD) spectra were recorded on a Jasco J-820 spectropolarimeter at 20 °C in 10 mM Na-phosphate buffer (pH 7.0) containing 1 mM Tris 2-carboxyethyl phosphine (TCEP) and 1% ethanol. The samples analyzed in a 10 mm optical path length cell were 1 μM rVDR-LBD proteins in the absence or presence of 5 μM $1,25(OH)_2D_3$. CD spectra in the region of 200 to 250 nm were obtained using a scanning speed of 20 nm/min, a time response of 1 s, a bandwidth of 1 nm, a data interval of 0.2 nm, and an average of four scans. Thermal transition curves were determined by monitoring the CD values at 222 nm as the temperature was increased by 1.0 °C/min from 20 to 85 °C.

Luciferrase Assays. COS-7 cells were cultured in Dulbecco's modified Eagle's medium supplemented with 5% fetal calf serum. Cells were seeded on 24-well plates at a density of 2×10^4 per well. After 24 h, the cells were transfected with a reporter plasmid containing three copies of the mouse osteopontin VDRE (SPPx3-TK-Luc), a mutant hVDR expression plasmid [pCMX-hVDR], and the internal control plasmid containing sea pansy luciferase expression constructs (pRL-CMV) by the lipofection method as described previously.[28] After 4 h of incubation, the medium was replaced with fresh DMEM containing 5% charcoal-treated FCS (HyClone, UT, USA). The next day, the cells were treated with either the ligand or ethanol vehicle and cultured for 24 h. Cells in each well were harvested with a cell lysis buffer, and the luciferase activity was measured with a luciferase assay kit (Toyo Ink, Inc., Japan). Transactivation measured by luciferase activity was normalized with the internal control. All experiments were done in triplicate.

Synthesis of Ligands. *General.* All nonaqueous reactions were carried out under argon or nitrogen in freshly distilled anhydrous solvents. We conducted high-pressure liquid chromatography (HPLC) by using Jasco 880-PU pumps equipped with an 801-SC solvent programmer and a Uvidec-100 V variable-length UV–vis detector. All samples for biological assays were purified by HPLC and shown to have a purity of >95% [YMC-Pack ODS-AM SH-342–5, 15–20% H_2O/MeOH, 8 mL/min]. Nuclear magnetic resonance (^1H and ^{13}C) spectra were recorded in $CDCl_3$ solution on a Bruker ARX 400 MHz spectrometer. Low (MS)- and high-resolution mass spectra (HRMS) were obtained by electronic ionization (70 eV) on a JEOL JMS-AX505HA spectrometer. Ultraviolet spectra were recorded on a Hitachi U-3200 spectrophotometer.

*1α-(tert-Butyldimethylsilyloxy)-25-(methoxymethoxy)-19-norvitamin D_3 3-Pivaloyl Ester (**7**) and 1α-(Pivaloyloxy)-25-(methoxymethoxy)-19-norvitamin D_3 3-(tert-butyl dimethylsilyl) Ether (**8**).* A 1.0 M THF solution of LiHMDS (912 μL, 0.912 mmol) was added to a solution of arylsulphone **5** (486.8 mg, 0.912 mmol) in THF (3 mL) at −78 °C, and the mixture was stirred for 30 min. A solution of ketone **6** (228.8 mg, 0.696 mmol) in THF (3 mL) was added to the mixture at −78 °C, the mixture was stirred for 1 h, and then the temperature was raised to −40 °C for 2 h. Saturated NH_4Cl solution was added to the reaction, the mixture was extracted with AcOEt, and the organic layer was washed with brine, dried over $MgSO_4$, and evaporated. The residue was chromatographed on silica gel and eluted with 2–3% AcOEt/hexane to give **7** and **8** (334.8 mg, 74%) as a 2:1 mixture and with 10% AcOEt/hexane to give **5** (187.1 mg, 38%). A mixture (2:1) of **7** and **8**: ^1H NMR ($CDCl_3$) δ 0.07 (6 H, s, Si-Me × 2), 0.53, 0.50 (2: 1) (3 H, s, H-18), 0.88–0.89 (9 H, s, Si-*t*Bu), 0.92 (3 H, d, J = 6.4 Hz, H-21), 1.15, 1.14 (2: 1) (9 H, s, CO*t*Bu), 1.22 (6 H, s, H-26, 27), 3.37 (3 H, s, OCH_3), 3.96 (1 H, m), 4.71 (2 H, s, OCH_2O), 5.08, 5.15 (2: 1) (1 H, m), 5.82, 5.71 (2: 1) (1 H, d, J = 11.2 and 11.5 Hz, H-7), 6.15, 6.23 (2: 1) (1 H, d, J = 11.2 and 11.5 Hz, H-6). Mass m/z (%) 646 (M^+, 0.1), 584 (0.4), 544 (11), 482 (100).

*1α-(tert-Butyldimethylsilyloxy)-25-(methoxymethoxy)-19-norvitamin D_3 (**9**) and 1α-Hydroxy-25-(methoxymethoxy)-19-norvitamin D_3 3-(tert-Butyldimethylsilyl) Ether (**10**).* A solution of DIBALH (441 μL, 0.441 mmol, 1.01 M toluene solution) was added to a solution of **7** and **8** (2:1 mixture, 95.2 mg, 0.147 mmol) in toluene (1 mL) at −78 °C and stirred for 1.5 h. The reaction was quenched by adding saturated sodium potassium tartrate, and the mixture was

dx.doi.org/10.1021/jm400537h | J. Med. Chem. 2013, 56, 6745–6760

extracted with AcOEt, and the extract was washed with brine, dried over $MgSO_4$, and evaporated. The residue was chromatographed on silica gel (5 g) and eluted with 10% AcOEt/hexane to give a 2:1 mixture of **9** and **10** (71.7 mg, 87%). The mixture was further chromatographed on fine silica gel (C-300, 5 g) and eluted with 5% AcOEt/hexane to give **9** (25.2 mg), a mixture of **9** and **10** (21.8 mg), and then **10** (10.7 mg). **9**: ^{1}H NMR ($CDCl_3$) δ 0.06, 0.07 (each 3 H, s, Si-Me × 2), 0.54 (3 H, s, H-18), 0.88 (9 H, s, Si-*t*Bu), 0.93 (3 H, d, J = 6.4 Hz, H-21), 1.22 (6 H, s, H-26, 27), 2.14–2.24 (2 H, m, H-4, 10), 2.47 (1 H, dd, J = 13.1, 3.2 Hz, H-4), 2.56 (1 H, dd, J = 13.0, 3.5 Hz, H-10), 2.80 (1 H, dd, J = 12.5, 4.2 Hz, H-9), 3.37 (3 H, s, OCH_3), 4.00 (1 H, m, H-1), 4.12 (1 H, m, H-3), 4.71 (2 H, s, OCH_2O), 5.84 (1 H, d, J = 11.2 Hz, H-7), 6.25 (1 H, d, J = 11.2 Hz, H-6). MS m/z (%) 562 (M^+, 9), 544 (8), 500 (62), 482 (83), 443 (32), 425 (42), 350 (42), 75 (100). **10**: ^{1}H NMR ($CDCl_3$) δ 0.06, 0.07 (each 3 H, s, Si-Me × 2), 0.54 (3 H, s, H-18), 0.87 (9 H, s, Si-*t*Bu), 0.93 (3 H, d, J = 6.4 Hz, H-21), 1.22 (6 H, s, H-26, 27), 2.14 (1 H, dd, J = 12.7, 7.7 Hz, H-4), 2.39 (1 H, dd, J = 13.1, 4.2 Hz, H-4), 2.41 (2 H, m, H-10, OH), 2.80 (1 H, dd, J = 12.1, 3.6 Hz, H-9), 3.37 (3 H, s, OCH_3), 4.04 (1 H, m, H-3), 4.11 (1 H, m, H-1), 4.71 (2 H, s, OCH_2O), 5.82 (1 H, d, J = 11.1 Hz, H-7), 6.27 (1 H, d, J = 11.1 Hz, H-6). MS m/z (%) 562 (M^+, 13), 500 (77), 482 (80), 443 (27), 425 (35), 350 (35), 75 (100).

*1α-(tert-Butyldimethylsilyloxy)-25-(methoxymethoxy)-19-norvitamin D_3 3-Methoxymethyl Ether (**11a**).* To a solution of **9** (53.7 mg, 0.095 mmol) in CH_2Cl_2 (400 μL) at 0 °C were added ethyldiisopropylamine (50.1 μL, 0.286 mmol) and MOMCl (14.5 μL, 0.191 mmol), and the mixture was stirred at room temperature for 3 h. HCl solution (1 N) was added to the reaction mixture, the mixture was extracted with CH_2Cl_2, and the extract was washed with 5% $NaHCO_3$ and brine, dried over $MgSO_4$, and evaporated. The residue was chromatographed on silica gel (4 g) and eluted with 10% AcOEt/hexane to give **11a** (50.6 mg, 87%), and then **9** was recovered (6.0 mg, 11%). **11a**: ^{1}H NMR ($CDCl_3$) δ 0.06 (6 H, s, Si-Me × 2), 0.54 (3 H, s, H-18), 0.87 (9 H, s, Si-*t*Bu), 0.93 (3 H, d, J = 6.4 Hz, H-21), 1.22 (6 H, s, H-26, 27), 2.22 (1 H, dd, J = 14.2, 7.3 Hz, H-4), 2.32 (1 H, dd, J = 13.4, 6.8 Hz, H-10), 2.43 (2 H, m, H-4, 10), 2.80 (1 H, dd, J = 12.4, 3.9 Hz, H-9), 3.36, 3.37 (each 3 H, s, OCH_3), 3.96, 4.06 (each 1 H, m, H-1, 3), 4.66, 4.68 (each 1 H, s, OCH_2O), 4.71 (2 H, s, OCH_2O), 5.83 (1 H, d, J = 11.3 Hz, H-7), 6.23 (1 H, d, J = 11.3 Hz, H-6). MS m/z (%) 606 (M^+, 31), 576 (39), 544 (96), 482 (92), 73 (100).

*1α-Hydroxy-25-(methoxymethoxy)-19-norvitamin D_3 3-Methoxymethyl Ether (**11b**).* To a solution of **11a** (77.0 mg, 0.127 mmol) was added TBAF (380.6 μL, 0.381 mmol), and the mixture was stirred for 3 h at room temperature. Then additional TBAF (190.3 μL, 0.190 mmol) was added, and the mixture was stirred for 5.5 h. The mixture was extracted with AcOEt, and the extract was washed with brine, dried over $MgSO_4$, and evaporated. The residue was chromatographed on silica gel (3.5 g) and eluted with 30% AcOEt to give **11b** (59.4 mg, 95%). **11b**: ^{1}H NMR ($CDCl_3$) δ 0.54 (3 H, s, H-18), 0.93 (3 H, d, J = 6.4 Hz, H-21), 1.22 (6 H, s, H-26, 27), 2.27 (1 H, dd, J = 13.4, 7.1 Hz, H-4), 2.36 (1 H, dd, J = 13.5, 7.0 Hz, H-10), 2.47 (1 H, dd, J = 13.4, 3.7 Hz, H-4), 2.61 (1 H, dd, J = 13.5, 3.6 Hz, H-10), 2.80 (1 H, dd, J = 12.3, 4.0 Hz, H-9), 3.36, 3.37 (each 3 H, s, OCH_3), 3.96 (1 H, m, H-3), 4.10 (1 H, m, H-1), 4.666, 4.669 (each 1 H, s, OCH_2O), 4.71 (2 H, s, OCH_2O), 5.84 (1 H, d, J = 11.2 Hz, H-7), 6.31 (1 H, d, J = 11.2 Hz, H-6). MS m/z (%) 492 (M^+, 21), 462 (29), 430 (98), 400 (59), 368 (100), 350 (18).

*1α-{(2-tert-Butyldimethylsilyloxy)-ethyloxy}-25-(methoxymethoxy)-19-norvitamin D_3 3-Methoxymethyl Ether (**13**).* To a solution of **11b** (24.0 mg, 0.0487 mmol) in DMF (500 μL) at 0 °C were added NaH (60% in oil, 58.4 mg, 0.293 mmol) and then bromide **12** (70.0 mg, 0.293 mmol), and the mixture was stirred 15 h at room temperature. The reaction was quenched by adding ice water and extracted with 50% AcOEt/hexane. The extract was washed with brine, dried over $MgSO_4$, and evaporated. The residue was chromatographed on silica gel (4 g) and eluted with 6% AcOEt/hexane to give **13** (6.0 mg, 19%) and then eluted with 8% AcOEt/hexane to give **11b** (4.7 mg, 16%). **13**: ^{1}H NMR ($CDCl_3$) δ 0.07 (6 H, s, Si-Me × 2), 0.54 (3 H, s, H-18), 0.89 (9 H, s, Si-*t*Bu), 0.93 (3 H, d, J = 6.4 Hz, H-21), 1.22 (6 H, s, H-26, 27), 2.28 (1 H, dd, J = 13.6, 6.6 Hz, H-4), 2.35 (1 H, dd, J = 13.6, 7.5 Hz, H-10), 2.44 (1 H, dd, J = 13.6, 3.5 Hz, H-4), 2.60 (1 H, dd, J = 13.6, 3.4 Hz, H-10), 2.80 (1 H, dd, J = 12.2, 3.7 Hz, H-9), 3.36, 3.37 (each 3 H, s, OCH_3), 3.53 (2 H, m, OCH_2), 3.72 (3 H, m, H-1, OCH_2), 3.96 (1 H, m, H-3), 4.66, 4.71 (each 2 H, s, OCH_2O), 5.85 (1 H, d, J = 11.2 Hz, H-7), 6.23 (1 H, d, J = 11.2 Hz, H-6). MS m/z (%) 650 (M^+, 5), 588 (7), 526 (3), 73 (100).

*1α-(2-Hydroxyethoxy)-25-hydroxy-19-norvitamin D_3 (**2a**).* CSA (12.8 mg, 0.055 mmol) was added to a solution of **13** (6.0 mg, 9.2 μmol) in MeOH (700 μL), and the mixture was stirred for 2.5 h at room temperature. Additional CSA (12.8 mg, 0.055 mmol) was added and stirred for 20 h. 5% $NaHCO_3$ was added to the reaction, and the mixture was extracted with AcOEt. The extract was washed with brine, dried over $MgSO_4$, and evaporated. The residue was chromatographed on silica gel (3.5 g) and eluted with 1% MeOH/AcOEt to give **2a** (2.9 mg, 71%). **2a**: ^{1}H NMR ($CDCl_3$) δ 0.54 (3 H, s, H-18), 0.94 (3 H, d, J = 6.4 Hz, H-21), 1.22 (6 H, s, H-26, 27), 2.23 (2 H, m, H-4, 10), 2.49 (1 H, dd, J = 13.5, 3.0 Hz, H-4), 2.73 (1 H, dd, J = 13.2, 3.4 Hz, H-10), 2.80 (1 H, dd, J = 12.5, 4.1 Hz, H-9), 3.59, 3.70 (2 H, 3 H, m, H-1, OCH_2 × 2), 4.13 (1 H, m, H-3), 5.85 (1 H, d, J = 11.2 Hz, H-7), 6.26 (1 H, d, J = 11.2 Hz, H-6). MS m/z (%) 448 (M^+, 100), 430 (74), 412 (10). UV λ_{max} (EtOH) 244, 252, and 262 nm.

*1α-{4-tert-Butyldimethylsilyloxy)butoxy}-25-(methoxymethoxy)-19-norvitamin D_3 3-(tert-Butyldimethylsilyl) Ether (**15**).* NaH (60% in oil, 41.8 mg, 1.04 mmol) and then tosylate **14** (60.2 mg, 0.168 mmol) in dry DMF (300 μL) were added to a solution of **10b** (19.6 mg, 0.035 mmol) in DMF (500 μL) at 0 °C, and the mixture was stirred for 15 h. The reaction was quenched by ice water and extracted with 50% AcOEt/hexane, and the extract was washed with brine, dried over $MgSO_4$, and evaporated. The residue was chromatographed on silica gel (4 g) and eluted with 5% AcOEt/hexane to give **15** (20.6 mg, 79%). **15**: ^{1}H NMR ($CDCl_3$) δ 0.04, 0.05, 0.06 (3 H, 3 H, 6 H, s, Si-Me × 4), 0.54 (3 H, s, H-18), 0.87, 0.89 (each 9 H, s, Si-*t*Bu × 2), 0.93 (3 H, d, J = 6.5 Hz, H-21), 1.22 (6 H, s, H-26, 27), 2.80 (1 H, m, H-9), 3.37 (3 H, s, OCH_3), 3.42, 3.62 (2 H, 3 H, m, H-1, OCH_2 × 2), 4.05 (1 H, m, H-3), 4.71 (2 H, s, OCH_2O), 5.83 (1 H, d, J = 11.2 Hz, H-7), 6.16 (1 H, d, J = 11.2 Hz, H-6). MS m/z (%): 748 (M^+, 5), 686 (50), 554 (13), 482 (73), 73 (100).

*1α-(4-Hydroxybutoxy)-25-hydroxy-19nor-vitamin D_3 (**2b**).* CSA (38.3 mg, 0.165 mmol) was added to a solution of **15** (20.6 mg, 0.027 mmol) in MeOH (600 mL), and the mixture was stirred at room temperature for 1 h. 5% $NaHCO_3$ solution was added, and the mixture was extracted with AcOEt. The extract was washed with brine, dried over $MgSO_4$, and evaporated. The residue was chromatographed on silica gel (3 g) and eluted with 1% MeOH/AcOEt to give **2b** (12.9 mg, 99%). **2b**: ^{1}H NMR ($CDCl_3$) δ 0.55 (3 H, s, H-18), 0.94 (3 H, d, J = 6.4 Hz, H-21), 1.22 (6 H, s, H-26, 27), 2.20 (1 H, dd, J = 13.3, 6.1 Hz, H-4), 2.26 (1 H, dd, J = 13.3, 8.1 Hz, H-10), 2.48 (1 H, dd, J = 13.3, 3.1 Hz, H-4), 2.69 (1 H, dd, J = 13.3, 3.5 Hz, H-10), 2.80 (1 H, dd, J = 12.3, 3.9 Hz, H-9), 3.48, 3.54 (each 1 H, OCH_2), 3.63 (3 H, m, H-1, OCH_2), 4.11 (1 H, m, H-3), 5.85 (1 H, d, J = 11.2 Hz, H-7), 6.26 (1 H, d, J = 11.2 Hz, H-6). MS m/z (%): 476 (M^+, 19), 458 (23), 386 (100), 368 (74). UV λ_{max} (EtOH): 244 nm, 252 nm, 262 nm.

*1α-(tert-Butyldimethylsilyloxy)-25-methoxymethoxy-2-spiro-[oxirane]-19-norvitamin D_3 (**17**).* To a solution of sulphone **5** (159.7 mg, 0.299 mmol) in THF (1 mL) at −78 °C was added a 1.0 M THF solution of LiHMDS (299 μL, 0.299 mmol). The mixture was stirred for 30 min at −78 °C, and then a solution of A ring ketone **16** (67.3 mg, 0.174 mmol) in THF (1.5 mL) was added. The mixture was stirred at −78 °C for 1 h, and then the temperature was raised to −10 °C during 2.5 h. A saturated NH_4Cl solution was added to the reaction, the mixture was extracted with AcOEt, and the extract was washed with brine, dried over $MgSO_4$, and evaporated. The residue was chromatographed on silica gel (6 g) and eluted with 2–3% AcOEt/hexane to give **17** (88.7 mg, 72%) as a mixture of epimers at C(2) and recovered **7** (30.3 mg, 19%). **17**: ^{1}H NMR ($CDCl_3$) δ 0.02–0.08 (12 H, s, Si-Me × 4), 0.55 (3 H, s, H-18), 0.86, 0.88 (each 9 H, s, Si-*t*Bu × 2), 0.94 (3 H, d, J = 6.4 Hz, H-21), 1.22 (6 H, s, H-26, 27), 2.75 and 2.82, 2.57, and 2.92 (3:2) (each 1 H, d, J = 5.5 Hz, $-CH_2OC-$), 3.37 (3 H, s, OCH_3), 3.68 (minor) (1 H, dd, J = 4.9, 2.8 Hz, H-1 or −3), 3.81, 3.88 (major) (each 1 H, dd, J = 7.0, 3.8 Hz, H-1

dx.doi.org/10.1021/jm400537h | J. Med. Chem. 2013, 56, 6745–6760

and −3), 4.04 (minor) (1 H, dd, J = 9.3, 4.6 Hz, H-1 or 3), 5.82 (1 H, d, J = 11.2 Hz, H-7), 6.21, 6.27 (3:2) (1 H, d, J = 11.2 Hz, H-6). MS m/z (%) 704 (M^+, 24), 642 (12), 585 (74), 73 (100).

*1α-Hydroxy-25-methoxymethoxy-2-spiro[oxirane]-19-norvitamin D_3 (**18**).* A 1.0 M THF solution of TBAF (377 μL, 0.377 mmol) was added to a solution of **17** (88.7 mg, 0.126 mmol) in THF (1 mL), and the mixture was stirred at room temperature for 4 h. The mixture was extracted with AcOEt, and the extract was washed with brine, dried over $MgSO_4$, and evaporated. The residue was chromatographed on silica gel (6 g) and eluted with 50% AcOEt/hexane to give 1,3-diol **18** (58.9 mg, 98%) as a mixture of epimers at C2. **18**: ^{1}HNMR ($CDCl_3$) δ 0.55 (3 H, s, H-18), 0.94 (3 H, d, J = 6.4 Hz, H-21), 1.22 (6 H, s, H-26, 27), 2.62, 2.72 (3:2) (1 H, dd, J = 13.6, 3.9 Hz), 2.85 and 3.08, 2.94, and 2.99 (3:2) (each 1 H, d, J = 4.7 Hz, $-CH_2OC-$), 3.37 (3 H, s, OCH_3), 3.81 (1 H, m, H-1 or −3), 3.91, 3.98 (3:2)(1 H, m, H-1 or −3), 4.71 (2 H, s, OCH_2O), 5.87 (1 H, m, H-7), 6.39 (1 H, m, H-6). MS m/z (%) 476 (M^+, 25), 414 (100).

*1α,2-Dihydroxy-25-(methoxymethoxy)-2-methyl-19-norvitamin D_3 (**19**).* $LiAlH_4$ (3.3 mg, 0.088 mmol) was added to a solution of diol **18** (20.9 mg, 0.044 mmol) in THF (500 μL), and the mixture was stirred at room temperature for 16 h. A solution of saturated potassium sodium tartrate was added to the reaction, and the mixture was extracted with AcOEt. The extract was washed with brine, dried over $MgSO_4$, and evaporated. The residue was chromatographed on silica gel (5 g) and eluted with 70% AcOEt/hexane to give triol **19** (17.2 mg, 82%) as a 3:2 mixture of epimers at C2. **19**: ^{1}H NMR ($CDCl_3$) δ 0.54 (3 H, s, H-18), 0.93 (3 H, d, J = 6.4 Hz, H-21), 1.22 (6 H, s, H-26, 27), 1.27, 1.30 (3:2) (3 H, s, H-2Me), 3.37 (3 H, s, OCH_3), 3.74 (2 H, m, H-1, 3), 4.71 (2 H, s, OCH_2O), 5.83 (1 H, m, H-7), 6.32 (1 H, m, H-6). MS m/z (%) 478 (M^+, 45), 416 (100), 398 (13).

*1α,2-Dihydroxy-25-(methoxymethoxy)-2-methyl-19-norvitamin D_3 2,3-Dimethyl Acetal (**20a**) and 1,2-Dimethyl Acetal (**20b**).* To a solution of triol **19** (34.6 mg, 0.072 mmol) in 2,2-dimethoxypropane (1 mL) was added TsOH·H_2O (1.4 mg, 7.23 μmol), and the mixture was stirred at room temperature for 1 h. The mixture was extracted with AcOEt, and the extract was washed with 5% $NaHCO_3$ and brine, dried over $MgSO_4$, and evaporated. The residue was chromatographed on silica gel (5 g) and eluted with 20% AcOEt/hexane to give **20** (28.4 mg, 64%) as a mixture of 2,3- and 1,2-diol acetonides (3:2). **20**: ^{1}H NMR ($CDCl_3$) δ 0.54, 0.55 (3:2) (3 H, s, H-18), 0.93 (3 H, d, J = 6.4 Hz, H-21), 1.22 (6 H, s, H-26, 27), 1.30, 1.34 (3:2) (3 H, s, H-2Me), 1.38, 1.45 (major) (each 3 H, s, $C\underline{(CH_3)_2}$), 1.39, 1.46 (minor) (each 3 H, s, $C\underline{(CH_3)_2}$), 3.37 (3 H, s, OCH_3), 3.88, 3.82 (3:2) (1 H, m, H-1 or −3), 4.04 (minor) (1 H, t, J = 4.1 Hz, H-1 or −3), 4.10 (major) (1 H, t, J = 4.4 Hz, H-1 or −3), 4.71 (2 H, s, OCH_2O), 5.78 (1 H, m, H-7), 6.26 (1 H, m, H-6). MS m/z (%) 518 (M^+, 97), 456 (100), 413 (11), 398 (33), 380 (23).

*1α-(2-tert-Butyldimethylsilyloxyethoxy)-2-hydroxy-25-(methoxymethoxy)-2-methyl-19-norvitamin D_3 2,3-Dimethyl Acetal (**22a**) and 1α,2-Dihydroxy-25-(methoxylmethoxy)-2-methyl-19-norvitamin D_3 3-(2-tert-Butyldimethylsilyloxyethyl) Ether 1,2-Dimethyl Acetal (**22a′**).* To a solution of alcohol **20** (11.8 mg, 0.028 mmol) in DMF (400 μL) were added NaH (60% in oil, 33.1 mg, 0.827 mmol) and a solution of tosylate **21a** (62.5 mg, 0.189 mmol) in DMF (500 μL). The mixture was stirred for 4 h at room temperature and then quenched with ice water. The mixture was extracted with 50% AcOEt/hexane, washed with brine, dried over $MgSO_4$, and evaporated. The residue was chromatographed on silica gel (5 g) and eluted with 5% AcOEt/hexane to give **22a** and **22a′** (11.8 mg, 63%) as a mixture (3:2) of isomers. **22a** and **22a′**: ^{1}H NMR ($CDCl_3$) δ 0.07, 0.05 (3:2)(6 H, s, Si-Me × 2), 0.54, 0.55 (3:2)(3 H, s, H-18), 0.90, 0.89 (3:2) (9 H, s, Si-*t*Bu), 0.93 (3 H, d, J = 6.4 Hz, H-21), 1.22 (6 H, s, H-26, 27), 1.325, 1.334 (3:2)(3 H, s, H-2Me), 1.37, 1.45 (major) (each 3 H, s, $C\underline{(CH_3)_2}$) 1.38, 1.47 (minor) (each 3 H, s, $C\underline{(CH_3)_2}$), 3.37 (3 H, s, OCH_3), 3.75−4.06 (6 H, m, H-1 and 3, $O\underline{(CH_2)_2}OTBS$), 4.71 (2 H, s, OCH_2O), 5.78 (1 H, m, H-7), 6.23 (1 H, m, H-6). MS m/z (%) 676 (M^+, 2), 614 (4), 599 (3), 556 (2), 438 (100).

*1α-(3-tert-Butyldimethylsilyloxypropoxy)-2-hydroxy-25-(methoxymethoxy)-2-methyl-19-norvitamin D_3 2,3-Dimethyl Acetal (**22b**) and 1α,2-Dihydroxy-25-(methoxylmethoxy)-2-methyl-19-norvitamin D_3 3-(3-tert-Butyldimethylsilyloxypropyl) Ether 1,2-Dimethyl Acetal (**22b′**).* Monohydroxy compound **20** (16.9 mg, 0.033 mmol) dissolved in DMF (900 μL) was treated with NaH (60% in oil, 52.0 mg, 1.30 mmol) and then tosylate **21b** (90.6 mg, 0.263 mmol) as in the synthesis of **22a** and **22a′**. The ethers **22b** and **22b′** (11.1 mg, 49%) were obtained after similar workup as a 3:2 mixture of isomers. **22b** and **22b′**: ^{1}H NMR ($CDCl_3$) δ 0.05, 0.04 (3:2) (6 H, s, Si-Me × 2), 0.54, 0.55 (3:2) (3 H, s, H-18), 0.89, 0.88 (3:2)(9 H, s, Si-*t*Bu), 0.93 (3 H, d, J = 6.4 Hz, H-21), 1.22 (6 H, s, H-26, 27), 1.32, 1.33 (3:2) (3 H, s, H-2Me), 1.37, 1.44 (major) (each 3 H, s, $C\underline{(CH_3)_2}$) 1.39, 1.47 (minor) (each 3 H, s, $C\underline{(CH_3)_2}$), 3.37 (3 H, s, OCH_3), 4.71 (2 H, s, OCH_2O), 5.78 (1 H, m, H-7), 6.21 (1 H, m, H-6).

*1α-(4-tert-Butyldimethylsilyloxybutoxy)-2-hydroxy-25-(methoxymethoxy)-2-methyl-19-norvitamin D_3 2,3-Dimethyl Acetal (**22c**) and 1α,2-Dihydroxy-25-(methoxylmethoxy)-2-methyl-19-norvitamin D_3 3-(4-tert-Butyldimethylsilyloxybutyl) Ether 1,2-Dimethyl Acetal (**22c′**).* Monohydroxy compound **20** (11.9 mg, 0.023 mmol) in DMF (700 μL) was similarly treated with NaH (60% in oil, 27.5 mg, 0.688 mmol) and tosylate **21c** (49.4 mg, 0.138 mmol). The ethers **22c** and **22c′** (10.6 mg, 65%) were obtained after similar workup as a mixture (3:2) of isomers. **22c** and **22c′**: ^{1}H NMR ($CDCl_3$) δ 0.05, 0.04 (3:2) (6 H, s, Si-Me × 2), 0.54, 0.55 (3:2) (3 H, s, H-18), 0.891, 0.887 (3:2) (9 H, s, Si-*t*Bu), 0.93 (3 H, d, J = 6.4 Hz, H-21), 1.22 (6 H, s, H-26, 27), 1.32, 1.33 (3:2)(3 H, s, H-2Me), 1.37, 1.45 (major) (each 3 H, s, $C\underline{(CH_3)_2}$), 1.39, 1.47 (minor) (each 3 H, s, $C\underline{(CH_3)_2}$), 3.37 (3 H, s, OCH_3), 3.39−3.70 (5 H, m, H-1 or 3, $O\underline{CH_2}(CH_2)_2\underline{CH_2}OTBS$), 4.00, 4.05 (3:2)(1 H, m, H-1 or 3), 4.71 (2 H, s, OCH_2O), 5.78 (1 H, m, H-7), 6.23 (1 H, m, H-6).

*1α-(2-Hydroxyethoxy)-2β,25-dihydroxy-2α-methyl-19-norvitamin D_3 (**2c**).* CSA (24.3 mg, 0.105 mmol) was added to a solution of **22a** and **22a′** (11.8 mg, 0.017 mmol) in MeOH (300 μL), and the mixture was stirred for 1.5 h at room temperature. Then, 5% $NaHCO_3$ was added to the reaction, and the mixture was extracted with AcOEt. The extract was washed with brine, dried over $MgSO_4$, and evaporated. The residue was chromatographed on silica gel (3 g) and eluted with 70% AcOEt/hexane to give a 3:2 mixture of regioisomers **2c** and **2c′** (7.2 mg, 87%). The mixture was separated by HPLC [YMC-Pack ODS-AM SH-342-5, 20% H_2O/MeOH, 8 mL/min] to give **2c** (2.59 mg, RT 21.08) and **2c′** (1.67 mg, RT 23.75). **2c**: ^{1}H NMR ($CDCl_3$) δ 0.54 (3 H, s, H-18), 0.94 (3 H, d, J = 6.4 Hz, H-21), 1.22 (6 H, s, H-26, 27), 1.29 (3 H, s, H-2Me), 2.37, 2.49 (each 1 H, m, H-4), 2.79 (1 H, dd, J = 12.6, 4.1 Hz, H-9), 2.91 (1 H, dd, J = 13.7, 4.4 Hz, H-10), 3.48−3.81 (6 H, m), 5.83 (1 H, d, J = 11.2 Hz, H-7), 6.26 (1 H, d, J = 11.2 Hz, H-6). MS m/z (%) 478 (M^+, 100), 460 (58), 442 (18). UV λ_{max} (EtOH): 244, 252, and 261 nm. **2c′** ^{1}H NMR ($CDCl_3$) δ 0.54 (3 H, s, H-18), 0.94 (3 H, d, J = 6.5 Hz, H-21), 1.22 (6 H, s, H-26, 27), 1.30 (3 H, s, H-2Me), 2.60 (1 H, dd, J = 13.7, 4.2 Hz), 2.73 (1 H, dd, J = 14.7, 5.5 Hz),2.79 (1 H, m), 3.55−3.74 (6 H, m), 5.81 (1 H, d, J = 11.1 Hz, H-7), 6.32 (1 H, d, J = 11.1 Hz, H-6). MS m/z (%) 478 (M^+, 100), 460 (55), 442 (24). UV λ_{max} (EtOH): 244 nm, 252 nm, 261 nm.

*1α-(3-Hydroxypropoxy)-2β,25-dihydroxy-2α-methyl-19-norvitamin D_3 (**2d**).* Deprotection of **22b** and **22b′** (11.1 mg, 0.016 mmol) by the procedure described above gave a 3:2 mixture of **2d** and **2d′** (4.3 mg, 54%). The mixture was separated by HPLC [YMC-Pack ODS-AM SH-342-5, 20% H_2O/MeOH, 8 mL/min to give **2d** (2.37 mg, RT: 20.18) and **2d′** (1.37 mg, RT: 21.60). **2d** ^{1}H NMR ($CDCl_3$) δ: 0.55 (3 H, s, H-18), 0.94 (3 H, d, J = 6.4 Hz, H-21), 1.22 (6 H, s, H-26, 27), 1.27 (3 H, s, H-2Me), 2.09 (1 H, dd, J = 13.1, 9.8 Hz, H-10), 2.36 (1 H, dd, J = 14.0, 5.2 Hz, H-4), 2.47 (1 H, m, H-4), 2.80 (1 H, dd, J = 12.3, 4.1 Hz, H-9), 2.89 (1H, dd, J = 13.7, 4.2 Hz, H-10), 3.44−3.86 (6 H, m), 5.83 (1 H, d, J = 11.2 Hz, H-7), 6.27 (1 H, d, J = 11.2 Hz, H-6). MS m/z (%) 492 (M^+, 100), 474 (65), 456 (26). UV λ_{max} (EtOH): 244, 252, and 261 nm. **2d′** ^{1}H NMR ($CDCl_3$) δ 0.55 (3 H, s, H-18), 0.94 (3 H, d, J = 6.5 Hz, H-21), 1.22 (6 H, s, H-26, 27), 1.25 (3 H, s, H-2Me), 2.60−2.81 (3H, m), 3.50−3.88 (6 H, m), 5.81 (1 H, d, J = 11.2 Hz, H-7), 6.32 (1 H, d, J = 11.2 Hz, H-6). MS m/z (%): 492 (M^+, 38), 474 (45), 456 (33), 135 (100). UV λ_{max} (EtOH): 244 nm, 252 nm, 262 nm.

*1α-(4-Hydroxybutoxy)-2β,25-dihydroxy-2α-methyl-19-norvitamin D_3 (**2e**).* Deprotection of **22c** and **22c′** (10.6 mg, 0.015 mmol) was similarly carried out by treatment with CSA (20.9 mg, 0.090

dx.doi.org/10.1021/jm400537h | J. Med. Chem. 2013, 56, 6745−6760

mmol) in THF/MeOH (1:1 400 μL) to give a 3:2 mixture of **2e** and **2e′** (4.6 mg, 60%). The isomers were separated by HPLC [YMC-Pack ODS-AM SH-342-5, 20% H_2O/MeOH, 8 mL/min] to give **2e** (3.68 mg, RT: 28.66) and **2e′** (0.90 mg, RT: 32.68). **2e** ^{1}H NMR ($CDCl_3$) δ 0.54 (3 H, s, H-18), 0.93 (3 H, d, *J* = 6.4 Hz, H-21), 1.22 (6 H, s, H-26, 27), 1.28 (3 H, s, H-2Me), 2.09 (1H, dd, *J* = 13.3, 9.7 Hz, H-10), 3.43–3.64 (2 H, OCH_2), 3.65–3.74 (4 H, m), 5.82 (1 H, d, *J* = 11.2 Hz, H-7), 6.26 (1 H, d, *J* = 11.2 Hz, H-6). Mass *m/z* (%) 507 (M^+, 6), 489 (4), 471 (1), 75 (100). UV λ_{max} (EtOH): 244 nm, 252 nm, 261 nm. **2e′** ^{1}H NMR ($CDCl_3$) δ 0.55 (3 H, s, H-18), 0.94 (3 H, d, *J* = 6.4 Hz, H-21), 1.22 (6 H, s, H-26, 27), 1.27 (3 H, s, H-2Me), 2.60–2.81 (3 H, m), 3.49 (2 H, OCH_2), 3.67 (3 H, m), 3.76 (1 H, m), 5.82 (1 H, d, *J* = 11.2 Hz, H-7), 6.31 (1 H, d, *J* = 11.2 Hz, H-6). MS *m/z* (%) 507 (M^+, 2), 489 (1), 75 (100). UV λ_{max} (EtOH): 244, 252, and 262 nm.

*5α-Butyl-1-(5-methoxymethoxy-1,5-dimethyl-hexyl)-7a-methyl-octahydro-inden-4-one (**24a**).* To a solution of iPr_2NH (706 μL, 5.04 mmol) in THF (10 mL) at −20 °C was added *n*-BuLi (2.8 mL, 4.37 mmol, 1.58 M hexane), and the mixture was stirred for 15 min. Grundman's ketone (1.09 g, 3.36 mmol) in THF (5 mL) was added to the LDA solution at −78 °C, the mixture was stirred for 1 h at that temperature, and then TMSCl (436 μL, 5.04 mmol) and Et_3N (702 μL, 5.04 mmol) were added. The temperature of the reaction was raised to −20 °C for 1.5 h. The solvent was evaporated, the residue was dissolved in hexane, and the mixture was passed through Celite to give **23** (1.34 g). To a solution of **23** (500.5 mg, 1.262 mmol) in THF (3 mL) at 0 °C was added MeLi (1.2 M Et_2O solution, 1.16 mL, 1.388 mmol) and stirred for 1 h. This solution of enolate was added to a solution of iodobutane (718 μL, 6.31 mmol) and HMPA (439 μL, 2.524 mmol) in THF (2 mL) at 0 °C, and the mixture was stirred at 0 °C for 3 h. A saturated NH_4Cl solution was added to the reaction, the solution was extracted with AcOEt, and the organic layer was washed with brine, dried over $MgSO_4$ and evaporated. The residue was chromatographed on silica gel (20 g) and eluted with 5% AcOEt/hexane to give **24a** (249.2 mg, 52%). **24a**: ^{1}H NMR ($CDCl_3$) δ 0.64 (3 H, s, H-18), 0.87 (3 H, t, J = 7.1 Hz, $(CH_2)_3\underline{CH_3}$), 0.95 (3 H, d, J = 6.1 Hz, H-21), 1.21 (6 H, s, H-26,27), 2.02 (1 H, m, H-9), 2.60 (1 H, dd, *J* = 11.6, 7.4 Hz, H-14), 3.37 (3 H, OMe), 4.70 (2 H, s, $O\underline{CH_2}O$). MS *m/z* (%) 380(M^+, 2), 365 (7), 318 (45), 227 (24), 262 (100), 219 (209, 103 (41).

*5-Butyl-1-(5-methoxymethoxy-1,5-dimethyl-hexyl)-7a-methyl-4-vinyl-octahydro-inden-4-ol (**25a**).* A solution of **24a** (303 mg, 0.80 mmol) in THF (3 mL) at 0 °C was treated with vinyl magnesium bromide (1.66 mL, 1.662 mmol THF solution), and the mixture was stirred for 3 h. The reaction was quenched by adding a 1 N HCl solution and extracted with AcOEt, and the organic layer was washed with brine, dried over $MgSO_4$, and evaporated. The residue was chromatographed on silica gel (5 g) and eluted with 10% AcOEt/hexane to give **25a** (297.5 mg, 88%). **25a**: ^{1}H NMR ($CDCl_3$) δ 0.88 (3 H, t, *J* = 7.1 Hz, $(CH_2)_3\underline{CH_3}$), 0.91 (3 H, d, *J* = 6.5 Hz, H-21), 0.96(3 H, s, H-189, 1.21 (6 H, s, H-26,27), 2.03 (1 H, m, H-14), 3.37 (3 H, s, OMe), 4.70 (2 H, s, OCH_2O), 5.02 (1 H, dd, *J* = 10.8, 1.6 Hz, H-6), 5.23 (1 H, dd, *J* = 17.2, 1.6 Hz, H-6), 5.94 (1 H, dd, *J* = 17.2, 10.8 Hz, H-7).

*[5-Butyl-1-(5-methoxymethoxy-1,5-dimethyl-hexyl)-7a-methyl-octahydro-inden-4-ylidene]-acetaldehyde (**26a**).* To a solution of **25a** (268.7 mg, 0.657 mmol) in CH_2Cl_2 (15 mL) was added PCC (723 mg, 3.288 mmol) and Celite (0.8 g), and the mixture was stirred at room temperature for 23 h. The reaction mixture was directly chromatographed on silica gel (10 g) and eluted with 5% AcOEt/hexane to give aldehyde **26a** (172.8 mg, 86%). **26a**: ^{1}H NMR ($CDCl_3$) δ 0.61 (3 H, s, H-18), 0.88 (3H, t, *J* = 7.2 Hz, $(CH_2)_3\underline{CH_3}$), 0.94 (3 H, d, *J* = 5.7 Hz,H-21), 1.21 (6 H, s, H-26,27), 2.36 (1 H, m, H-14), 3.37 (3 H, s, OMe), 3.39 (1 H, m, H-9), 4.71 (2 H, s, OCH_2O), 5.78 (1 H, d, *J* = 8.3 Hz, H-7), 10.06 (1 H, d, *J* = 8.3 Hz, CHO).

*2-[5-Butyl-1-(5-methoxymethoxy-1,5-dimethyl-hexyl)-7a-methyl-octahydro-inden-4-ylidene]-ethanol (**26b**).* $NaBH_4$ (13.9 mg, 0.367 mmol) in EtOH (2 mL) was added to a solution of aldehyde **26a** (200.5 mg, 0.493 mg) in EtOH (1.5 mL) at 0 °C, and the mixture was stirred for 1 h. Water was added to the reaction, and the mixture was extracted with AcOEt, and the extract was washed with brine, dried over $MgSO_4$, and evaporated. The residue was chromatographed on silica gel (10 g) and eluted with 20–25% AcOEt/hexane to give **26b** (172.8 mg, 86%). **26b**: ^{1}HNMR ($CDCl_3$) δ 0.56 (3 H, s, H-18), 0.88 (3 H, t, *J* = 7.3 Hz, $(CH_2)_3\underline{CH_3}$), 0.94 (3 H, d, *J* = 6.4 Hz, H-21), 1.21 (6 H, s, H-26,27), 2.12 (1 H, m, H-14), 2.62 (1 H, m, H-9), 3.37 (3 H, s, OMe), 4.15, 4.25 (each 1 H, m, H-6), 4.71 (2 H, s, OCH_2O), 5.23 (1 H, m, H-7). MS e/z (%) 408 (M^+, 0), 346 (11), 328 (58), 313 (23), 271 (19), 243 (33), 217 (100).

*5-Butyl-4-[2-(diphenyl-phosphinoyl)-ethylidene]-1-(5-methoxy-methoxy-1,5-dimethyl-hexyl)-7a-methyl-octahydro-indene (**27**).* To a solution **26b** (156 mg, 0.382 mmol) in THF (2 mL) at 0 °C were added a solution of *n*-BuLi (1.58 M hexane, 266 μL, 0.420 mmol) and then a solution of TsCl (87.4 mg, 0.458 mmol) in THF (0.2 mL), and the mixture was stirred for 5 min. In another flask, to a solution of diphenylphosphine (133 μL, 0.764 mmol) in THF (1 mL) at 0 °C was added a solution of *n*-BuLi (1.58 M hexane, 484 μL, 0.764 mmol) to yield a red solution. This red solution was slowly added via a double headed needle to the above solution of tosylate until the red color did not disappear in the solution, and the mixture was stirred for 30 min. Water (20 μL) was added to the reaction, and the solvent was evaporated. The residue was dissolved in CH_2Cl_2 (2 mL) and cooled to 0 °C, 10% H_2O_2 (3 mL) was added to this solution, and the mixture was stirred at 0 °C for 1 h. Sodium thiosulfate (2 N) was added to the reaction, the mixture was extracted with CH_2Cl_2, and the organic layer was washed with brine, dried over $MgSO_4$, and evaporated. The residue was chromatographed on silica gel (8 g) and eluted with 40% AcOEt/hexane to give Wittig–Horner reagent **27** (173.7 mg, 77%). **27**: ^{1}H NMR ($CDCl_3$) δ 0.23 (3 H, s, H-18), 0.86 (3 H, t, *J* = 7.4 Hz, $(CH_2)_3\underline{CH_3}$ overlapped with H-21), 1.20 (6 H, s, H-26,27), 2.02 (1 H, m, H-14), 2.49 (1 H, m, H-9), 2.98, 3.34 (each 1 H, m, H-6), 3.36 (3 H, s, OMe), 4.70 (2 H, s, OCH_2O), 5.04 (1 H, m, H-7), 7.43–7.78 (10 H, m, aromatic H). MS *m/z* (%) 592 (M^+, 2), 530 (100), 473 (33), 419 (4), 216 (74), 202 (91).

*9α-Butyl-1α-(tert-butyldimethylsilyloxy)-25-methoxymethoxy-19-norvitamin D_3 3-(tert-Butyldimethylsilyl) Ether (**29**).* To a solution of phosphine oxide **27** (124.1 mg, 0.209 mmol) in THF (2 mL) at −78 °C were added HMPA (36 μL, 0.209 mmol) and *n*-BuLi (1.58 M hexane solution, 132 μL, 0.209 mmol), and the mixture was stirred for 15 min. To this solution was slowly added ketone **28** (37.5 mg, 0.105 mmol) in THF (1 mL), the mixture was stirred for 1 h at −78 °C, and then the temperature of the reaction was slowly raised to room temperature, and the mixture was stirred at room temperature for 3 h. The reaction was quenched by adding saturated NH_4Cl and extracted with AcOEt, and the organic layer was washed with brine, dried, and evaporated. The residue was chromatographed on silica gel (8 g) and eluted with 2% AcOEt/hexane to yield **29** (15.7 mg, 21%, 81% on the basis of recovered **27**) and then eluted with 40% AcOEt/hexane to give starting phosphine oxide **27** (91.3 mg, 74%). **29**: ^{1}H NMR ($CDCl_3$) δ 0.048, 0.053 (each 6H, s, SiMe), 0.54 (3 H, s, H-18), 0.865, 0.87 (each 9H, s, $\underline{t}$-BuSi overlapped with $(CH)_2\underline{CH_3}$), 0.92 (3 H, d, *J* = 6.3 Hz, H-21), 1.21 (6 H, s, H-26,27), 2.83 (1 H, m),3.37 (3 H, s, OMe), 4.71 (2 H, s, OCH_2O), 4.07 (2 H, m, H-1,3), 5.83 (1 H, d, *J* = 11.2 Hz, H-7), 6.14 (1 H, d, *J* = 11.2 Hz, H-6).

*9α-Butyl-1α,25-dihydroxy-19-norvitamin D_3 (**4a**).* To a solution of **29** (28.5 mg, 0.039 mmol) in MeOH (1 mL) was added CSA (54.2 mg, 0.233 mmol), and the mixture was stirred for 1.5 h at room temperature. A 5% $NaHCO_3$ solution was added to the reaction, the solution was extracted with AcOEt, and the extract was washed with brine, dried over $MgSO_4$, and evaporated. The residue was chromatographed on silica gel (4 g) and eluted with 70% AcOEt/hexane to give **4a** (17.2 mg, 96%). Since **4a** contains a minor product, it was purified by HPLC (YMC-Pack ODS-AM SH-342-5, 15% H_2O/MeOH, 8 mL/min) to yield **4a** (11.8 mg) and its geometrical isomer **4a′** (1.0 mg) at the 7-position. **4a**: ^{1}H NMR ($CDCl_3$) δ 0.54 (3 H, s, H-18), 0.87 (3 H, t, 7.2 Hz, $(CH_2)_3\underline{CH_3}$), 0.93 (3 H, d, *J* = 6.4 Hz, H-21),1.22 (6 H, s, H-26,27), 2.82 (1 H, m, H-9), 4.07 (2 H, m, H-1,3), 5.87 (1 H, d, *J* = 11.2 Hz, H-7), 6.31 (1 H, d, *J* = 11.2 Hz, H-6). UV (EtOH) λ_{max} (ε) 244 (27,000), 252 (31,000) and 261 nm (21,000). MS z/e (%) 460 (M^+, 21), 442 (100), 424 (36), 406 (15), 331 (31), 313 (32), 295 (21). **4a′** [(7Z)-9α-Butyl-1α,25-dihydroxy-19-norvita-

dx.doi.org/10.1021/jm400537h | J. Med. Chem. 2013, 56, 6745–6760